CORSO DI DOTTORATO DI RICERCA IN
BIOLOGIA MOLECOLARE CELLULARE E AMBIENTALE

XXX CICLO

"EXTRA-RIBOSOMAL ROLE OF RPS19 IN NORMAL AND TUMOR CELL LINES EXPOSED TO IONIZING RADIATIONS"

PhD Student: Antonella Longo

Tutor: Prof. Antonio Antoccia

PhD School Coordinator: Prof. Paolo Mariottini

53BP1 53 Binding Protein 1

AMPK AMP-activated protein Kinase

ATM Ataxia Telangiectasia Mutated Protein

ATR Ataxia Telangiectasia and RAD3 related protein

DBA Diamond-Blackfan Anemia

DDR DNA Damage Response

DNA-PK DNA Dependent Protein Kinase

DSBs Double Strand Breaks

eEF2 Elongation Factor 2

eEF2K Elongation Factor 2 Kinase

HR Homologous Recombination

HSP90 Heat Shock Protein 90

IR Ionizing Radiation

IRIF Ionizing Radiation Induced Foci

MDM2 Murine Double Minute 2

mTORC1 Mammalian Target of Rapamycin Complex 1

NHEJ Non Homologous End Joining

p21 cyclin-dependent kinase inhibitor 1

p-ATM ph-Ser1981-ATM

p-CHK2 ph-Thr68-CHK2

p-eEF2 ph-Thr56-eEF2

p-p53 ph-Ser15-p53

p-RPS6 ph-Ser240/244-RPS6

RPs Ribosomal Proteins

RPS19 Ribosomal Protein S19

SSBs Single Strand Breaks

VP16 Etoposside

γ-H2AX ph-Ser139-H2AX

1. RIASSUNTO

La biogenesi del ribosoma eucariotico è un processo finemente regolato che si realizza nel nucleolo e richiede l'attività coordinata di tutte e tre le RNA polimerasi (Pol): Pol I trascrive il precursore dell'RNA ribosomale (rRNA) 45S/47S che è processato in 28S, 18S e 5.8S; Pol II trascrive 80 mRNA che saranno poi tradotti in Proteine Ribosomali (RPs), mentre Pol III trascrive l'rRNA 5S. Una volta mature, le RPs saranno assemblate con gli rRNA maturi per formare la piccola (40S) e la grande (60S) subunità ribosomale, le quali compongono il funzionale ribosoma eucariotico 80S [1]. Qualsiasi alterazione nel processo di biogenesi ribosomale induce una condizione cellulare denominata "Stress Ribosomale". Rari disordini genetici, chiamati "Ribosomopatie", sono associati a questa condizione cellulare [2]. Uno di questi è la Diamond-Blackfan anemia (DBA), causata principalmente da mutazioni nel gene codificante per *RPS19* [3]. La DBA, chiamata anche "anemia dell'infanzia", è un disordine dovuto ad anemia, macrocitosi reticolocitopenia e diminuzione o assenza di precursori eritroidi nel midollo osseo [4]. Inoltre, essa è caratterizzata da eritropoiesi difettose e da anomalie fisiche, come bassa statura e difetti cardiaci [5]. La DBA è stata associata a suscettibilità alle Radiazioni Ionizzanti (IR) [6] ed ad un maggiore rischio di sviluppare tumori, come leucemia mieloide acuta, sarcoma osteogenica, sindrome mielodisplastica e tumori solidi [4, 7].
La condizione di stress ribosomale induce l'attivazione del tumor soppressore p53, il quale attiva proteine a valle come p21/CDKN1A (p21), capace di controllare il ciclo cellulare [8]. p53 è un fattore coinvolto anche nella risposta al danno al DNA (DNA Damage Response, DDR). Esposizioni a IR o trattamenti con composti radiomimetici favoriscono lesioni al doppio filamento del DNA (Double Strand Breaks, DSBs), le quali possono essere risolte attraverso due vie di riparazione attivate in relazione al ciclo cellulare: Non Homologous End Joining (NHEJ), attivata principalmente durante la fase del ciclo cellulare G0/G1 e Homologous Recombination (HR), attivata in fase S e G2 del ciclo cellulare in cui è disponibile il DNA duplex [9]. La via di riparazione NHEJ richiede la presenza dell'eterodimero KU70/KU80 che, insieme al fattore DNA-PKcs, interviene come sensore per riconoscere e legare DSBs. Nella via di segnalazione HR il sensore di danno è il complesso MRN, composto dalle proteine MRE11, RAD50 e NBN. Il "fattore chiave" è la chinasi ATM, attivata mediante auto-fosforilazione sul residuo Ser1981 e seguente monomerizzazione [10]. Una volta attivata, ATM fosforila una gruppo di proteine a valle come H2AX, 53BP1, CHK2, p53, RAD51, RAD52 che

conducono la cellula verso la riparazione del DNA, l'arresto del ciclo cellulare o l'apoptosi.
Negli ultimi anni alcuni studi hanno evidenziato il ruolo extra-ribosomale di alcune RPs, coinvolte in diversi processi cellulari. Il nostro obiettivo è stato studiare la connessione tra la condizione di stress ribosomale e l'attivazione della risposta al danno al DNA; in particolare, identificare il ruolo extra-ribosomale di RPS19 nel danno al DNA indotto dall'esposizione a IR.
Gli esperimenti sono stati eseguiti in fibroblasti primari umani MRC-5, cellule di glioblastoma U251-MG e cellule tumorali di colon HCT116. La condizione di stress ribosomale è stata indotta attraverso la trasfezione transiente di siRNA contro la proteina ribosomale S19 (iRPS19); come controllo, ogni linea cellulare è stata trasfettata con siRNA scramble (iSCR). La maggior riduzione dei livelli proteici di RPS19, ottenuta usando 15 nM di siRNA, è stata osservata 48 e 72 ore dopo la trasfezione nelle cellule tumorali e nei fibroblasti rispettivamente. Inoltre, il danno del DNA è stato causato utilizzando la dose di 5 Gy di raggi X.
La condizione di stress ribosomale riduce il tasso di sintesi proteica, bloccando la fase di allungamento della traduzione. Il tasso di sintesi proteica è stato valutato mediante il livello di fosforilazione dei fattori RPS6 e di eEF2, rispettivamente regolatore positivo e negativo della fase di allungamento del processo di traduzione. Il livello di fosforilazione RPS6 è invariato dopo il trattamento con raggi X, sia durante stress ribosomale sia nelle cellule di controllo. Al contrario, eEF2 è iper-fosforilato a partire da 8 ore nelle cellule iRPS19 ed a 24 ore nelle cellule di controllo.
Uno dei principali fattori alterati dalla condizione di stress ribosomale è p53, proteina fondamentale nella salvaguardia del genoma.
In cellule iRPS19, l'esposizione a IR determina la stabilizzazione di p53 dopo 16 ore; mentre la sua attivazione è osservata come risposta a lungo termine, come descritto dal livello proteico del suo target molecolare p21. Il maggiore livello proteico di p21 è osservato a 24 ore dopo aver indotto danno al DNA. Tuttavia le analisi FACS non descrivono alcuna alterazione del ciclo cellulare, mentre il saggio di BrdU mostra la riduzione del numero di MRC-5 e HCT116 in fase S in seguito ad esposizione a raggi X.
Il trattamento con IR attiva la via di risposta DDR. Pertanto ho analizzato diversi fattori coinvolti in questa via di segnalazione in concomitanza con la condizione di stress ribosomale utilizzando analisi di western blot, tecniche di immunofluorescenza ed analisi qRT-PCR. Le cellule iRPS19 irraggiate mostrano alterazioni nella cinetica di attivazione dei fattori γ-H2AX e 53BP1: il numero dei foci di entrambi i marcatori aumenta soprattutto nella fase iniziale di attivazione. Secondo i dati ottenuti, la nostra condizione

sperimentale altera anche la chinasi ATM. Nonostante il livello totale della proteina ATM non sia modificato, il suo livello di fosforilazione Ser1981 in cellule iRPS19 è massimo a 2 ore ed alti livelli sono presenti fino a 8 ore dopo l'esposizione a raggi X. La risposta HR richiede l'attivazione di proteine MRE11, RAD50 e NBN. Sia i livelli proteici totali sia il numero di foci formati sono inalterati in cellule iRPS19 esposte a raggi X. Una volta attivata, la chinasi ATM fosforila diversi fattori a valle, compreso CHK2 sul residuo Thr68. Nelle cellule HCT116 deplete di RPS19, il livello di p-Thr68-CHK2 segue quello di p-Ser1981-ATM. Infatti, p-Thr68-CHK2 è rapidamente attivato ed è presente fino a 8 ore dopo l'esposizione, punto sperimentale in cui il livello torna a livello basale nelle cellule di controllo iSCR. I fibroblasti e le cellule di glioblastoma non mostrano la stessa regolazione. Tra i fattori a valle della chinasi ATM è presente p53, che può essere direttamente fosforilato sul residuo Ser15. Il livello di fosforilazione di p53 è alterato solamente in cellule U251-MG deplete di RPS19. Come descritto per p-Ser1981-ATM, il livello di p-Ser15-p53 è massimo a tempi brevi, ma è presente fino a 24 ore dopo l'esposizione a raggi X. Al contrario i fibroblasti e cellule tumorali di colon non mostrano alcuna alterazione nel livello p-Ser15-p53, né in seguito alla deplezione di RPS19 né come risposta al trattamento con IR.

Poiché la riparazione tramite HR richiede l'attività della proteina RAD51, sono stati valutati possibili alterazioni legate alla deplezione di RPS19 ed in seguito a IR. Nonostante la condizione di stress ribosomale non alteri i livelli trascrizionali di RAD51, i dati ottenuti dimostrano una forte riduzione del suo livello proteico. In cellule iRPS19, il livello proteico di RAD51 è ulteriormente ridotto dopo l'esposizione a raggi X, così come il numero di foci formati sui siti di danno del DNA. Tuttavia, l'analisi di co-immunoprecipitazione non descrive alcuna interazione diretta tra RPS19 e RAD51, evidenziando quindi che i livelli proteici di RAD51 non sono direttamente dipendenti dalla presenza di RPS19. Tra gli interattori di RAD51 è stato identificato lo chaperone molecolare HSP90, il cui livello proteico è invariato sia in seguito a deplezione di RPS19 sia ad esposizione a raggi X. Inoltre, il livello di RPS19 è costante dopo il trattamento con 17AAG, inibitore dell'attività ATPasica dello chaperone. Infine monitorando il fattore KU80, sono state analizzate possibili alterazioni della via di riparazione NHEJ. Il livello proteico di KU80 non è modificato né in seguito a deplezione di RPS19 né a trattamento con raggi X.

In conclusione, i dati raccolti hanno dimostrato che, in seguito ad esposizione a IR, la deplezione di RPS19 altera alcuni fattori coinvolti nella DDR, in particolare RAD51, fattore chiave nella via di riparazione HR.

2. SUMMARY

Eukaryotic ribosome biogenesis is a highly regulated process that takes place into nucleolus and requires the coordinated activity of all the three RNA-polymerases (Pol). Pol I transcribes the precursor ribosomal RNA (rRNA) 45S/47S that is processed into the 28S, 18S and 5.8S; Pol II transcribes 80 mRNAs that will be translated in Ribosomal Proteins (RPs), whereas Pol III transcribes the rRNA 5S. Once matured, RPs will be assembled with mature rRNAs to form the small (40S) and the large (60S) ribosomal subunits that compose the functional eukaryotic ribosome 80S [1]. Any alteration in the ribosome biogenesis process induces a cellular condition named "Ribosomal Stress". Rare genetic disorder, named "Ribosomopathies", are associated to this cellular condition [2]. One of these is the Diamond-Blackfan Anemia (DBA) and it's caused by mutations mainly in gene encoding for *RPS19* [3]. DBA is a congenital erythroid aplasia characterized by defective erythropoiesis [4] and physical abnormalities, such as short stature and cardiac defects [5]. DBA revels sensitivity to Ionizing Radiation (IR) [6] and a major risk to develop cancer, such as acute myeloid leukemia, osteogenic sarcoma, myelodysplastic syndrome and solid tumors [4, 7].

Ribosomal stress condition induces the activation of tumor suppressor p53, which in turn activates downstream proteins such as p21/ CDKN1A (p21) able to check cell cycle [8]. p53 is also a factor involved in DNA damage response (DDR). IR or radiomimetic drugs induce DNA Double Strand Breaks (DSBs) that can be resolved through two pathways activated in relation to cell cycle: Non Homologous End Joining (NHEJ), mainly activated during G0/G1 cell cycle phase and Homologous Recombination (HR), activated both in the middle and late S and in G2 cell cycle phases in which DNA duplex is available [9]. The NHEJ requires KU70/KU80 heterodimer and DNA-PKcs factor, as sensors to recognize and bind DSBs. In HR mechanism the DNA damage sensor is the MRN complex composed by MRE11, RAD50 and NBN proteins. Key player is ATM kinase which is activated via auto-phosphorylation at Ser1981 and consequent monomerizzation [10]. Once activated, ATM phosphorylates a plethora of downstream proteins including H2AX, 53BP1, CHK2, p53, RAD51, RAD52. The effects of these factors are to induce the cells toward DNA repair, cell cycle arrest or apoptosis.

In the last years several researches have highlighted the extra-ribosomal role of some RPs involved in different cellular mechanisms. Our aim was to investigate the relationship between "Ribosomal Stress" conditions and the

activation of DDR; in particular to identify the extra-ribosomal role of RPS19 in DNA damage caused by IR exposure.
Experiments were performed in normal human primary fibroblasts MRC-5, glioblastoma cells U251-MG and colon cancer cells HCT116. Ribosomal stress condition was induced through siRNA transfection against RPS19 (iRPS19); as control, each cell lines was transfected using a control siRNA scramble (iSCR). In each cell line, the highest RPS19 knockdown, observed at using 15 nM of siRNA concentration, was obtained 48 and 72 hours after transfection in cancer cells and fibroblasts respectively. Moreover, DNA damage was induced using 5 Gy of X-Rays.
Ribosomal stress condition reduces protein synthesis process blocking the elongation phase of translation. The protein synthesis process was evaluated by monitoring the phosphorylation levels of RPS6 and eEF2 proteins, respectively positive and negative regulators of elongation phase of translation. The phosphorylation of RPS6 was not affected by IR, both in absence and in presence of RPS19. On the other hand, eEF2 iper-phosphorylation was observed starting from 8 hours in iRPS19 and 24 hours in iSCR cells.
One of the main factors altered by the ribosomal stress condition is p53, key player in the preservation of the genome.
RPS19-depleted cells showed p53 stabilization mainly 16 hours after IR, while its activation, described by its molecular target p21, was observed as long term response to damage. Indeed, p21 highest amount was detected at 24 hours. However FACS analysis described no alteration in any phase of cell cycle, while BrdU assay highlighted the reduction of number of HCT116 and MRC-5 cells able to enter in S phase after X-Ray exposure.
IR treatment activates DDR pathways, thus I focused on analysis of factors involved in DDR using western blot, immunofluorescence staining and qRT-PCR analysis.
RPS19-depleted and irradiated cells displayed alteration in γ-H2AX and 53BP1 activation: the number of foci formation increased mainly in the early phase of activation, in both analyzed markers. Collected data showed that our experimental condition altered also ATM kinase. Despite ATM total protein level was unchanged, its phosphorylation was deregulated in iRPS19 irradiated cells. In each iRPS19 cell lines, the highest p-Ser1981-ATM protein level was observed at 2 hours and slowed down to return basal, in fact it was detectable until 8 hours after treatment. DDR requires the activation of MRE11, RAD50 and NBN sensor proteins. MRN complex total protein levels and foci formation were unaltered in iRPS19 irradiated cells. Once activated, the kinase ATM phosphorylates downstream factor,

including CHK2 on Thr68. Only HCT116 iRPS19 irradiated cells described alteration of CHK2 phosphorylation, as well as p-Ser1981-ATM. Indeed, p-Thr68-CHK2 protein was rapidly activated and was recorded until 8 hours, in which it returned to basal level in iSCR radiated cells. Fibroblasts and glioblastoma iRPS19 cells did not show deregulation. Among ATM kinase downstream factors is present p53, which can be directly phosphorylated on Ser15. P-Ser15-p53 level was altered in U251-MG iRPS19 cells, as well as p-Ser1981-ATM. Indeed, p-Ser15-p53 protein level enhanced at 4 hours and its amount was progressively reduced until recovery the basal level in 24 hours after treatment. Fibroblasts and colon cancer cells did not describe p-Ser15-p53 level alteration as response to IR, both in presence and in absence of RPS19.

HR repair pathway requires the activity of RAD51 protein for strand invasion and repair DNA lesions. Nevertheless, RAD51 transcription level did not change, ribosomal stress condition induced a strong reduction of RAD51 protein level. In iRPS19 cells, RAD51 total protein level was further reduced after IR, as the number of foci detected on DNA damage sites. Moreover, co-immunoprecipitation analysis did not show a direct interaction between RAD51 and RPS19 factors, describing that RAD51 protein level reduction was not directly dependent by RPS19.

Among RAD51 interactors it has been identified HSP90, which total protein level was unaltered in iRPS19 irradiated cells. Furthermore RPS19 protein level was not affected after the inhibition of HSP90 ATPase activity, performed by 17-AAG treatment.

Finally, a possible NHEJ impairment was evaluated by KU80, which protein level was not affected both in ribosomal stress and in response to IR.

In conclusion, data collected have demonstrated that, in response to IR, RPS19 depletion affects some factors involved in DDR, in particular RAD51, key player in HR repair pathway.

3. INTRODUCTION

3.1 Eukaryotic ribosome biogenesis

Eukaryotic ribosome biogenesis is a highly regulated process that takes place into the nucleolus, a specialized compartment within the nucleus. This process requires the coordinated activity of all the three RNA-polymerases: the RNA polymerases I,II and III. The RNA polymerase enzymes have to be coordinated to ensure high efficiency and an accurate ribosome production. RNA polymerase I (Pol I) synthesizes the precursor rRNA 45S/47S, which, once matured, forms the major ribosomal RNA (rRNA) represented by 28S, 18 and 5.8S rRNA [11]; RNA polymerase II (Pol II) synthesizes the mRNAs that will be translated in Ribosomal Proteins (RPs), the most of small nuclear RNA and microRNAs [12]; RNA polymerase III (Pol III) synthesizes transfer RNAs (tRNA), ribosomal RNA (rRNA) 5S and other small RNAs [13]. The matured eukaryotic ribosome is named 80S and is composed by the large subunit (60S) and the small subunit (40S). To produce the ribosome 80S, four rRNAs and about eighty RPs are necessary. RPs mRNAs are translated into the cytoplasm and then imported into the nucleolus to be assembled with mature rRNAs. In detail, the rRNA 28S, 5.8S, 5S and 47 RPs compose the large (60S) ribosomal subunit; while rRNA 18S and 32 RPs compose the small one (40S). The pre-40S subunit is processed in the cytoplasm, whereas the maturation of the pre-60S starts into nucleus and is completed into cytoplasm (Fig. 1). To have a correct synthesis, maturation and export of 80S ribosome are require nearly 200 non ribosomal factors [14]. Therefore, formation of eukaryotic ribosomes requires the coordination of processing, assembly events and also a spatio-temporal organization of each steps between the nucleolus and the cytoplasm.

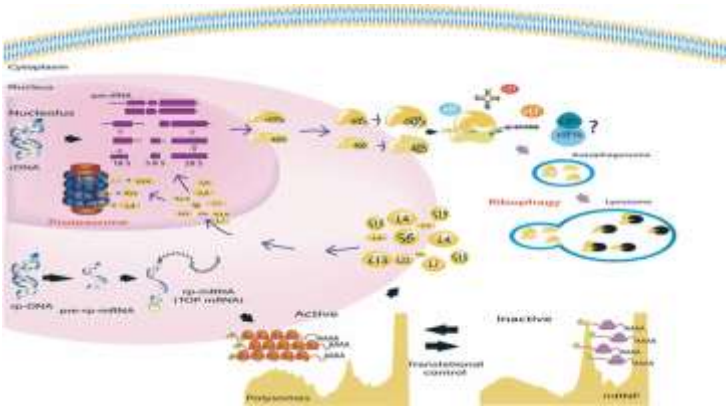

Fig.1 Ribosome biogenesis [1]
RPs mRNAs are translated into the cytoplasm and then imported into the nucleolus to be assembled with mature rRNAs into two ribosomal subunits. The 40S and 60S subunits are then exported into the cytoplasm to form matured eukaryotic ribosomes 80S.

3.2 Ribosomal stress and protein synthesis

Any kind of alteration in ribosome biogenesis induces a cellular condition named “Ribosomal Stress” or “Nucleolar Stress”. For example, ribosomal stress condition can be due to loss of RPs, defects in assembly or export in ribosomal components, defects in rRNAs production and maturation.
One of the main cellular response to ribosomal stress condition is the reduction in protein synthesis, a highly regulated process, responsive to growth and stress stimuli in order to link mRNA translation activity to the cell metabolic demands. This process is ruled by mTORC1 (Mammalian Target Of Rapamycin Complex 1) complex both in initiation and in elongation phase (Fig. 2). The initiation phase is mainly checked through 4EBP1 (eIF4E-binding protein 1), while elongation phase through the activity of p70S6K1. P70S6K1 promotes the process allowing the phosphorylation of eEF2K (Elongation Factor 2 Kinase) on Ser366, negative regulator of eEF2 (Elongation Factor 2). The Thr56 residue of eEF2 is an important site of phosphorylation, since it defines the elongation phase of translation process: if it is ipo-phosphorylated allows a correct elongation rate, otherwise its iper-phosphorylation blocks the process. Nevertheless the specific activity of mTORC1 is not altered during

ribosomal stress condition [15], the level of total protein synthesis process is reduced because of level of the inhibitory phosphorylation of eEF2. Indeed, eEF2K is more active in myelogenous leukemia K562C and in colon cancer HCT116 RPS19-depleted cells, as well as in PC3 cells with low levels of RPS6, RPS7 or RPS19. This condition leads to the iper-phosphorylation of eEF2 and the consequent inhibition of elongation phase of translation [16].

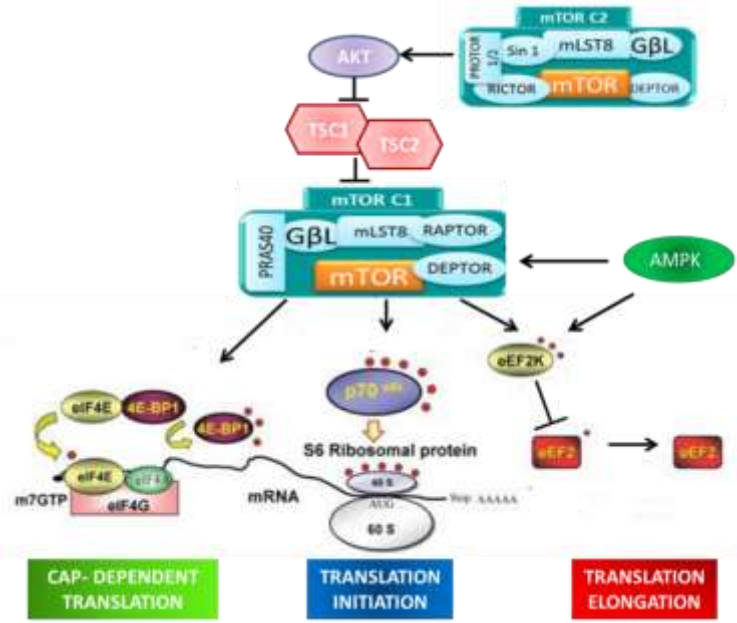

Fig. 2 Regulation of protein synthesis process (modified by **[17])**
Overview of translation process. In response to different cellular stress, mTORC1 complex checks different phase of protein synthesis process.

3.3 Ribosomal stress diseases and Diamond-Blackfan Anemia

Ribosomal stress condition is associated to specific pathological conditions named "Ribosomopathies" [2], rare genetic disorders characterized by macrocytic anemia associated to growth retardation and development of physical abnormalities. However, the feature most represented is the failure of erythropoiesis [18, 19]. The clinical ribosomopathies most known are: Diamond-Blackfan Anemia (DBA), 5q- Syndrome, Treacher Collins

Syndrome (TCS), Shwachman Diamond Syndrome (SDS), Cartilage hair hypoplasia (CHH), Dyskeratosis Congenita (DKC), Common variable immunodeficiency (CVID), Turner syndrome.
DBA is a congenital erythroid aplasia characterized by defective erythropoiesis and physical abnormalities, such as short stature and cardiac defects [5]. DBA revels sensitivity to X-Rays [6] and major risk to develop cancer, in particular acute myeloid leukemia (AML), osteogenic sarcoma, myelodysplastic syndrome and solid tumors (ST) [4, 7]. However, the exact risk for cancers associated with DBA is not known yet. DBA is mainly expressed in infancy and actually patients are treated with steroids care. About 25-50% of DBA cases are familiar [20] and 25% of case are associate with mutations in the gene encoding for *RPS19*, located on chromosome 19. *RPS19* gene is the most mutated, in fact it have been identified base mutations, insertions or deletions. Furthermore, up to 50% of DBA patients display mutations in other RPs genes [21]: different studies have shown the presence of mutations also in genes encoding for *RPL5* (6.6%), *RPL11* (4.8%), *RPL35A* (3%), *RPS24* (2%), *RPS17* (1%), and *RPS7* (<1%) [2] (Fig. 3). Since all DBA patients are heterozygous for RPs allele, it can be assumed that the disease is caused by haploinsufficiency or dominant negative effect of the mutated genes. Furthermore, the reduction of RPs could lead to impairment of the formation of mature 80S ribosome, which may be the main cause of this specific pathogenesis [22, 23]**.**

Disease	Gene	Mutations	Molecular phenotype	Phenotype	Cancer association
Diamond Blackfan Anemia (DBA)	RPS19 25% RPS24 2% RPS17 1% RPL35A RPL11 RPL5	27 small deletions and insertions; 25 missense; 14 splice site defects; 13 nonsense; 7 large deletions and rearrangements	mRNA levels reduction (30%); protein levels reduction (20%); ribosomal association defect (20%); unclassified (30%) **haploinsufficiency and/or dominant negative effect**	physical anomalies: craniofacial, thumb, cardiac, urogenital; red cell aplasia	solid tumor (colon adenocarcinoma; osteogenic sarcomas; breast cancers; squamous cell carcinomas) AML; MDS; radiosensibilty

Fig. 3 Diamond-Blackfan Anemia mutation (modified by**[24])**
Partial overview of the mutated RPs in DBA.

3.4 The extra-ribosomal functions of ribosomal proteins

The main role of RPs is to allow a correct production and ribosome function. However, in the last years, new functions of RPs have been discovered; in fact RPs not associated to ribosome, as in ribosomal stress condition, can have different and specific extra-ribosomal functions [25]. It has been demonstrated that RPs can be involved in different cellular processes and are able to rule specific pathways in order to mediate different cellular responses. In particular, RPs can be involved in processes as DNA repair, apoptosis, cell cycle block, cell proliferation, development and differentiation, neoplastic transformation, cell migration and invasion (Fig. 4) [26-28].

Extraribosomal functions	RPs
Apoptosis	S3, S3a, S6, S7, S14, S25, S27, S27L, S29, L3, L6, L7, L8, L23, L26
Cell cycle	S3, S5, S6, S7, S14, S15, S19, S20, S25, S26, S27, S27L, S27a, L3, L5, L6, L7, L11, L13, L23, L26, L31, L34, L37, L41
Cell proliferation	S6, S9, S13, S14, S15a, S24, S27, L6, L8, L11, L15, L17, L26, L29, L31, L34, L36a
Neoplastic transformation	S3a, S14, L5, L22, L41
Cell migration and invasion	S3, p-S6, S7, S15a, S24, S27, L15

Fig. 4 Extra-ribosomal role of Ribosomal Proteins [29]
A simplified overview of the extra-ribosomal role of RPs.

In detail evidences have been collected on:

DNA Repair: one of the identified extra-ribosomal role of RPs regards DNA repair process [30]. The 7,8-dihydro-8-oxoguanine (8-oxoG) residues in DNA can be recognized by RPS3 which, interacting with a base excision repair enzyme (OGG1), promotes its catalytic activity. Moreover, RPS3 is able to binds p53 and protects it from MDM2 (Murine Double Minute 2) mediated degradation [31]; so RPS3 is involved in maintaining the genomic integrity. In addition, RPL3 over-expression increases phospho-H2AX amount after ribosomal biogenesis impairment caused by 5-FU and L-OHP in human pulmonary adenocarcinoma Calu-6 and human colon cancer HCT116 p53-/- cells, meaning that RPL3 is able to increase DNA damage [32].

Furthermore, RPS19 deficient human $CD34^+$ fetal liver cells show p53 activation and stabilization because of its phosphorylation at residues Ser15 and Ser37 by kinases as ATR, ATM, CHK1 and CHK2 [33-35].
In addition, RPS19 deficient zebrafish show high levels of factors involved in activation of the ATR/ATM-CHK1/CHK2/p53 pathway, such as phospho-H2AX and phospho-CHK1 [36].
During ribosomal stress, RPs deficient cells increase demand for rDNA, resulting in hyper-activation of rDNA units; in addition, defects in transcription [37] and in mRNA splicing increase the formation of DNA Double-Strand Breaks (DSBs) [38]. Moreover, RPs deficient cells catabolize the defective rRNA, produce more nucleotides and increase the amount of dNTPs pool, leading to dNTPs pool imbalance which can be a source of DNA damage [39-41]. This mechanism results in changes of expression of enzymes involved in nucleotide metabolism. In fact, RPS19 deficient zebrafish cells display high levels of ATP and AMPK (AMP-activated protein Kinase) phosphorylation at residue Thr172. Activated AMPK can phosphorylate p53 on Ser15 and activates energy saving measures in the cells, such as inhibition of translation process [36].

Apoptosis: after irreparable damage cells can activate apoptosis process to induce cell death and to guarantee the genomic integrity. It has been shown that some RPs have a role in apoptosis process, both as positive and as negative regulators. As positive regulators it can be identified RPS3[42] and RPS29 [43] able to induce apoptosis in a caspase-dependent manner; RPS6, in its unphosphorylated form, promotes DR4 expression in TRAIL-induced cell death [44], RPL3 and RPL7 exhibit pro-apoptotic activity [45]. In contrast RPS27 knockdown induces apoptosis through the inhibition of NF-κB (Nuclear Factor κ chain transcription in B cells) activity [29] and RPL23 expression promotes primary multidrug resistance (MDR) in gastric cancer cells by suppressing drug-induced apoptosis [46]. Thus, RPs are able to promote or inhibit apoptosis process depending on different stress cellular conditions.

Regulation of Development and Differentiation: RPs play a role in embryonic development [47]. RPS7 deficient zebrafish embryos show development defects in hematopoiesis and abnormalities in the brain [48]. RPS19 knockdown causes embryonic lethality in mice [49], while RPL22 deficiency blocks the development of T cells inducing their death [50]. Down-regulation of the RPs levels during retinoic acid induced neuronal differentiation has also been observed. RPL29 deficiency leads to

osteogenesis and bone marrow fragility in mice and promotes cellular differentiation [51]. The depletion of RPS9 in glioma cells impairs 18S rRNA production, allowing morphological differentiation in a p53-dependent manner [52]. The inactivation of RPS5 leads to the erythroid differentiation of murine erythroleukemia (MEL) cells while RPS5 overexpression induces MEL cells differentiation [53].

Cell migration and invasion: RPs not associated to ribosome play a role in cell migration and invasion processes acting during the initiation, progression and in the late phase of tumorigenesis. Iper-phosphorylation of RPS6 is associated with metastatic tumors [54]: RPS3, RPS15A and RPS24 are identified as positive regulator of carcinogenesis [28]. On the other hand RPS27, RPL15 and RPS7 can inhibit cells migration and invasion [28, 55]. Nevertheless it is supposed that RPs can contribute to neoplastic transformation and cancer progression, this specific extra-ribosomal role remains to be elucidated.

Regulation of Angiogenesis: Angiogenesis is crucial for cancer development and progression. The loss of RPL29 expression reduces the VEGF (Vascular Endothelial Growth Factor)-stimulated microvessel formation [56].

Cell cycle arrest and cell proliferation: RPs can indirectly check cell cycle regulation both in p53-dependent and -independent pathways. Many RPs, including RPS3, RPS7, RPS14, RPS15, RPS20, RPS25, RPS26, RPS27, RPS27a, RPL5, RPL6, RPL11, RPL23, RPL26, and RPL37 were reported to activate p53 and to induce p53-dependent cell cycle arrest in an indirect manner [29]. In addition, some of above mentioned RPs such as RPS6 [57], RPS19 [58] and RPL7 [56] can induce cell cycle arrest also in a p53-independent manner.

3.5 P53-dependet pathway in response to ribosomal stress

One of the main cellular response to ribosomal stress condition results in p53 stability, suggesting that the nucleolus is a central hub for stress sensors [59]. The p53 tumor suppressor regulates the expression of many downstream target genes. In order to protect cells from transformation and tumorigenesis, p53 downstream genes check processes such as cell cycle arrest, apoptosis, DNA repair and senescence in response to stress of

various nature [60]. Thus p53 becomes essential for maintaining the genomic stability during cell growth and division. The main regulator of p53 is the MDM2, an E3 ubiquitin-protein ligase [61]. MDM2 protein has three well-defined regions: the N-terminus for p53 binding, a central region that contains acidic and zinc finger domains and a C-terminal RING finger domain which possesses the ubiquitin ligase region [62]. In normal cells the p53 level is maintained low through MDM2-p53 negative loop. p53 activates MDM2 transcription which, in turn, inactivates p53 through its ubiquitination and proteasomal degradation [63]. p53 protein level increases in response to various stress condition, such as ribosomal stress. In this context, some of the RPs not associated to mature ribosome 80S are able to move from the nucleolus into the nucleoplasm where can bind MDM2 (Fig. 5). For example RPL11 [64], RPL23 [65], RPL5 [66] and RPS7 [67] have been shown to bind the zinc finger domain of MDM2, preventing MDM2-mediated degradation of p53. More recently, several investigations have discovered new RPs able to modulate the MDM2-p53 pathway, such as RPL6, RPL26, RPS3, RPS7, RPS14, RPS25, RPS26, RPS27 and RPS27 [29].

Although the effect of above mentioned RPs is the same, each of them show a different way to mediate the same cellular response. For example RPL26 can bind the 5′-UTR of p53 mRNA, promoting the increase of p53 translation in response to DNA damage [68], RPS3 can interact directly with p53 and protect it from MDM2 ubiquitination in response to oxidative stress [31].

Nevertheless the list of RPs able to bind MDM2 is still growing, no data has been yet reported about RPS19. However, erythroblasts deficient in RPS19 show modest stabilization of p53 with consequent p21/CDKN1A (p21) increase [69], as well as in primary bone marrow-derived $CD34^+$ cells [70]. Moreover, RPS19 depletion increases p53 level in colon cancer HCT116, prostate cancer LNCaP and 22RV1 and breast cancer MCF7 cells [71].

So an imbalance in RPs concentrations induces p53 accumulation, stabilization and activation, leading to alterations in cell cycle progression and apoptosis. Therefore, beside their fundamental role for the correct assembly of 80S, RPs have an important role as regulators of ribosomal stress condition pathways [72].

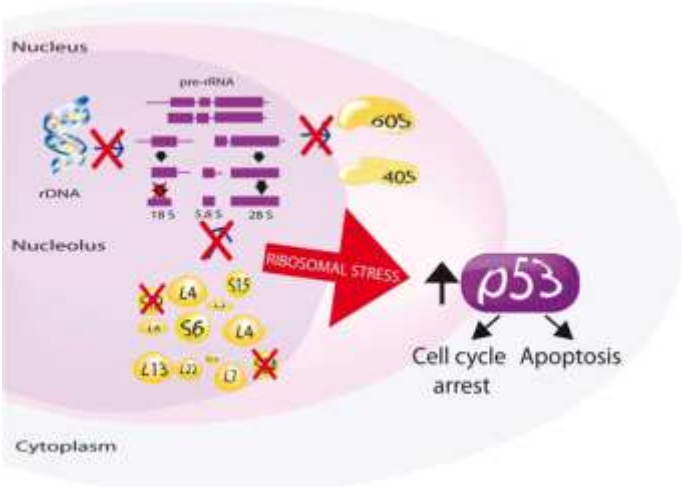

Fig. 5 p53 activation in response to ribosomal stress condition [1]
Defects in ribosome biogenesis lead to activation of tumor suppressor p53 which can block cell cycle or promote apoptosis.
Red crosses indicate some steps that may induce ribosomal stress condition.

3.6 P53-independet pathway in response to ribosomal stress

Ribosomal stress conditions can induce cellular response also in a p53-independent pathway. It has been demonstrated that RPL11 can rule the oncogene c-Myc and to induce its mRNA degradation or the inhibition of downstream genes expression [73]. RPL3 can activate p21, checking cell cycle and apoptosis in a p53-independent manner [45]. RPS27 is able to promote DNA repair and apoptosis preventing GADD45α (growth arrest and DNA damage inducible gene *GADD45α*) ubiquitination [74]. The p53-independent pathway can be ruled also by factors which act in association with RPs. For example, the kinase PIM1 (Proviral Integration site for Moloney murine leukemia virus 1), associated with RPS19, is able to drive cell cycle progression and to reduce cell proliferation in absence of p53 [58].

3.7 Ribosomal stress and cell cycle

Ribosomal stress condition induces the stabilization and the activation of p53, major regulator of cell cycle control both in G1/S and in G2/M transition. This cellular response is mainly caused by free RPs but also defects in factors involved in ribosome biogenesis can be responsible, for example nucleolin [75], nucleophosmin [76] and nucleostemin [77]. It has been demonstrated that the extra-ribosomal role of specific RPs is linked to progression of cell cycle or apoptosis, via p53-dependent and independent mechanisms. Some RPs induce direct and indirect activation of p53, so are able to block cell cycle progression.

For example, both RPL5 and RPL11 are necessary for the accumulation of p53 and the consequent G1 arrest [47]; RPS13 promotes G1 arrest through down-regulation of cyclin-dependent kinase inhibitor p27 expression and CDK2 (Cyclin-Dependent Kinase 2) activity [46], while RPL34 inhibits CDK4 (Cyclin-Dependent Kinase 4) resulting in G1 arrest. Abnormal expression levels of RPL7 and RPL32 arrest cell cycle and promote apoptosis, while RPS19 knockdown is characterized by accumulation in G1. G0/G1 arrest after RPS19 depletion has been reported in erythroid TF-1 or in human haematopoietic cells $CD34^+$ [78], in erythroblasts and in chronic myelogenous leukemia K562 cells [79].

RPS19 depletion results in G1/S cell-cycle delay also in mouse fetal liver cells [69] and in zebrafish [80, 81].

In addition, DBA erythroid cells expressing low level of RPS19 arrest at the G0/G1 phase of the cell cycle [82], as well as primary fibroblasts of DBA patients with RPS19 acceptor splice site mutation (c.72-2A>C) [83].

On the other hand some RPs promote cell proliferation. For example, it has been demonstrated that RPS15A knockdown induces cell cycle arrest at G0/G1 phase [84], effect observed also after depletion of RPL26 and RPL29 [29, 85].

It suggests that RPs not bounded to 80S ribosome can indirectly check cell cycle.

3.8 DNA damage, DNA damage response and repair process

DNA transmits genetic information into the progeny of cells and organisms. Its primary structure can be subjected to alterations by cellular processes such as DNA replication, repair and recombination. DNA integrity can be compromised also by endogenous cellular metabolites and exogenous DNA-damaging agents, both of chemical and physical nature. Any kind of

alteration at DNA structure, if not repaired or miss-repaired, might cause mutations at gene or at chromosomal level. Different forms of genotoxic agents, as reactive oxigen species (ROS), exposure to ultraviolet light (UV) and Ionizing Radiation (IR), lead to DNA lesions of different nature which can be resolved by activation different DNA damage response (DDR) pathways (Fig. 6) able to solve DNA lesions and restore the integrity of the DNA sites or induce apoptosis process in order to eliminate heavily damaged cells.

Exposure to IR causes many types of DNA damage, as oxidized bases, DNA-protein crosslink, Single and Double Strand Breaks (SSBs, DSBs) [86-88].

In this context DSBs represent the most dangerous lesions [89] and are solved through Homologous Recombination (HR) (Fig. 7) and Non Homologous End joining (NHEJ) (Fig. 8) repair pathways.

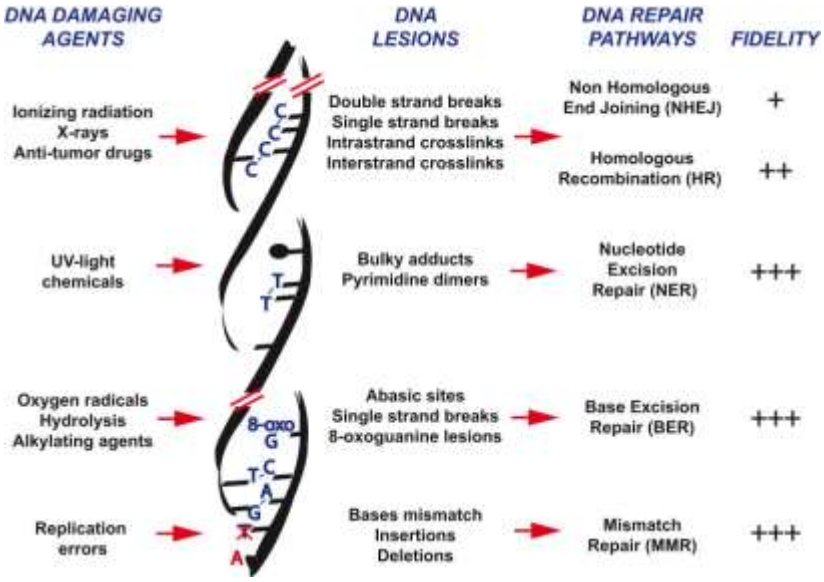

Fig. 6 DNA-Repair Pathways in Mammalian Cells [90]

DNA-induced damage triggers a cascade of signals and subsequent repair mechanisms involving several unique and overlapping factors.

The distinguishing property of HR is that the information lost from the broken duplex is rescued from a homologous duplex, in fact it is an error-free mechanism of repair. HR pathway is mainly present during the late S phase and the S/G2. HR consists in three main steps: strand invasion, branch migration and the resolution of Holliday junction formation. After DNA damage, the histone H2AX changes in the chromatin structure, becoming exposed [9]. The structural modification permits the recruitment of ATM/ATR/DNA-PKcs complex which causes a rapid phosphorylation of the histone H2AX in the DNA regions flanking the breaks. The kinase ATM (Ataxia Telangiectasia Mutated protein) is the first factor recruited on DNA damage site. ATM is a 350kD nuclear serine/threonine protein that belongs to PIKK (Phosphatidylinositol 3-Kinase-related Kinases) family, which comprises also ATR (Ataxia Telangiectasia and RAD3 related protein) and DNA-PKcs (DNA dependent protein kinase) proteins. DNA damage promotes ATM activation by rapid autophosphorylation on Ser367, Ser1893, Ser1981 and consequent monomerizzation [91]. In turn, ATM monomers are able to recruit and activate several DNA Damage Response (DDR) proteins. The first factor phosphorylated is H2AX which, phosphorylated on Ser139 (γ-H2AX), forms specific sites named foci or IRIF (Ionizing Radiation Induced Foci) [92, 93]. γ-H2AX foci becomes a platform of recruitment for all proteins involved in DDR, such as 53BP1(53 Binding Protein 1) [94, 95]. The first complex recruited is MRN composed by MRE11, RAD50 and NBN proteins, which make a nucleolytic resection of the DSBs in the 5'–3' direction. The 3' single-stranded DNA is then recognized by RAD complex, formed by RAD51, RAD52, RAD54 and other proteins [9]. RAD52 interacts with RAD51 [96] and promotes its activity [97], while RPA, interacting with RAD52 [98], stabilizes RAD51 at DNA strand [99]. Thus, RAD51 starts the strand invasion in order to change the undamaged DNA duplex with damaged DNA strand. The specific structure composed is named D-loop and is then resolved by MUS81-MMS4 (Fig. 7).

Several studies have demonstrated a mechanism of control in HR linked to p53 activity, since it interacts with some proteins implicated in HR including BLM, BRCA1, BRCA2, RAD52 and RAD51 [100]. For example, p53 can control RAD51 activity by the binding of its functional domain, highly conserved and located between amino acids 125 and 220 [101]. Moreover, after Etoposide treatment, p53 binds *RAD51* promoter resulting in down-regulation of RAD51 mRNA and protein and in inhibition of RAD51 foci formation [102].

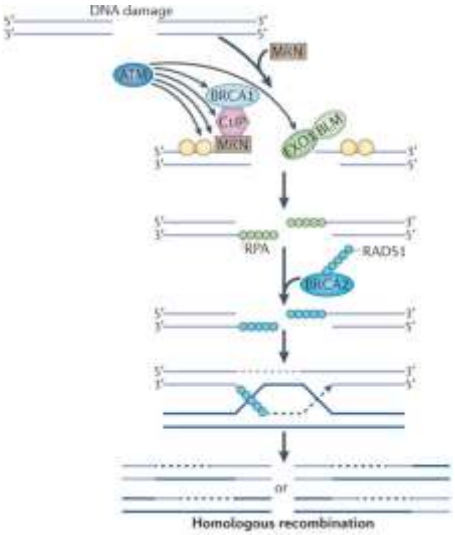

Fig. 7 Homologous Recombination repair systems (modified by **[103])**
A simplified overview of HR pathway, activated to repair DSBs.

The NHEJ system ligates the two ends of a DSBs without the requirement of sequence homology between DNA ends. NHEJ pathway is mainly activated in the G1 phase, so is an error-prone repair pathway which alters the original DNA sequence at the damaged sites: in fact it is associated with additions/deletions of nucleotides at the generated junctions. The NHEJ pathway consists in DSBs recognition, procession of the damaged DNA ends to remove non-ligable groups and restore the DNA strands. The first step in NHEJ is the binding of a heterodimeric complex composed by KU70/KU80. The KU complex binds the damaged site in order to create the scaffold for the assembly of all NHEJ enzymes and to protect the DNA from exonuclease digestion. Once bound to DNA lesions, KU70/KU80 heterodimer changes its conformation becoming able to recognize the catalytic subunit of DNA-PKcs [10]. DNA-PKcs binds the carboxy-terminus of the KU complex in a specific structure, forming an active DNA-PKcs holoenzyme [104]. DNA-PKcs, a serine/threonine kinase, regulates its activity through autophosphorylation that allows its dissociation from DNA ends. Thus, DNA-PKcs can activate a plethora of downstream factors, such as RPA2, WRN, Cernunnos/XLF, LigIV and XRCC4 [105], an important

DNA–PKcs target [106]. The last step of NHEJ requires the formation of XRCC4-ligase IV complex, able to bind DNA ends and drive their link, carrying out DNA repair process (Fig. 8). However the XRCC4–ligase IV complex is unable to ligate DSBs not processed yet. In this context two locally processed DNA ends are joined through the coordinated action of the LigIV/XRCC4/XLF factors and the DNA-PKcs complex [105, 107]. Another protein involved in processing overhangs during NHEJ is the protein Artemis, which can form a complex with DNA-PKcs and shows single-strand-specific exonuclease activity [108]. Other proteins are involved in the reaction depending on the chemistry of the lesions. Moreover, new proteins involved in NHEJ repair pathway are not still discovered.

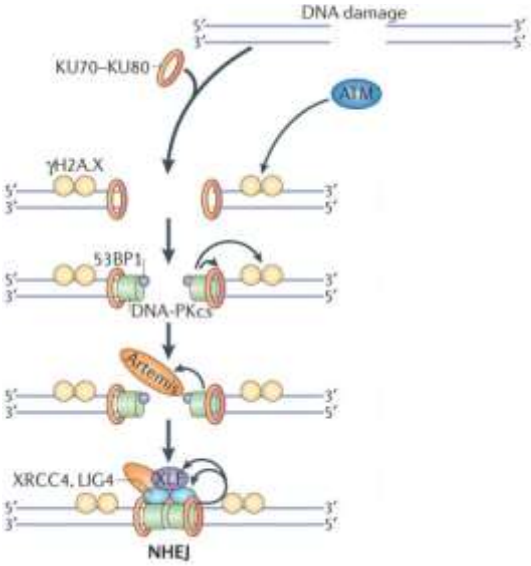

Fig. 8 Non Homologous End Joining repair systems (modified by **[103])**
A simplified overview of NHEJ, activated to repair DSBs.

After DNA damage both ATR and ATM kinases can check cell cycle by p53. In particular ATR [109] and ATM [110] can cause p53 stabilization and activation through direct phosphorylation on Ser15, crucial event to enhance p53 transcriptional activity [110].
ATM can block cell cycle also via ATM-CHK2-Cdc25A axis. In this context, ATM phosphorylates Thr68 of its downstream factor CHK2 [111], which in turn phosphorylates p53 on Ser20 [109, 112]. This phosphorylation blocks p53/MDM2 interaction leading to p53 stabilization [109, 113]. Ser20 residue can be phosphorylated also by ATR-CHK1-Cdc25A axis [109].
ATM shows a third control measure on p53 stability through direct phosphorylation of M2M2 on Ser395 [114]. This modification blocks MDM2/p53 interaction, inhibiting p53 export and degradation [114].
Once stabilized, p53 can activate its molecular target as p21, able to inhibit the S phase and to cause G1/S arrest [115, 116].
Furthermore, CHK2 can induce cell cycle block by promoting the phosphorylation of Cdc25A phosphatase, which prevents the activation of cyclin-CDK complexes and mitosis-promoting factors. This condition leads to cell cycle arrest during G2/M transition, as well as phosphorylation of BRCA2 (Breast Cancer Type 2) on Ser329, regulator of RAD51 activity. Indeed, BRCA2 level is high in G2/M and reduced in G1 phase [117].
The competition between HR and NHEJ depends also by the presence of homologous chromosome, which is available starting from S phase. Indeed, HR factors act coping information from homologous chromosome, thus, with the progression of S phase, HR becomes the main pathway required for DNA repair (Fig. 9).
Also the initial binding of repair factors to the DNA breaks may affect “the choice” of DDR signaling, as occurs during the S and G2 phases in which both pathway can be activated. For example, the KU70/KU80 heterodimer can be recruited to DSBs more quickly than HR factors [118], leading to reduction of HR activation; while RAD52 competes with the KU complex for the binding to DNA ends, resulting in reduction of NHEJ activation.
Several studies have reported alterations in DDR pathways as consequence of ribosomal stress condition. However, no data have been collected about effects of IR in RPs-depleted or mutated cells.
In response to DSBs caused by Etoposide, RPS19-depleted zebrafish cells show phosphorylation of different HR proteins such as p53 on Ser15 and Ser37, ATM Ser1981, 53BP1 Ser1778, CHK1 Ser345 and CHK2 Thr68 [36].

Moreover, RPS26 regulates p53 activity in response to DSBs caused by Doxorubicin treatment, in HCT116 RPS26-depleted cells. Doxorubicin do not affect p53 level but significantly impaired up-regulation of p21 and MDM2 because of defects in p53 acetylation and in the binding of target genes promoters. In addition, Doxorubicin induces cell cycle arrest at G2/M instead of G1 phase, in IMR90 and HCT116 RPS26-depleted cells [85]. Furthermore the same compound causes RPL37 degradation, as occur in response to intrastrand crosslinks induced by Cisplatin treatment [119].
Also RPL3 is able to influence HR and NHEJ repair pathways; in particular it shows strong effects in inhibiting the NHEJ [32] and it is able to colocalize with SSBs induced by oxidative stress [120].
Finally, RPS27a mRNA level in immortalized human hepatocyte (IHH) cells increases both in response to DSBs caused by Etoposide and after SSBs caused by UV light. In particular, Etoposide treatment causes p53 recruitment on *RPS27a* gene, resulting in *RPS27a* promoter acetylation and consequent increase of RPS27a protein half-life [121].

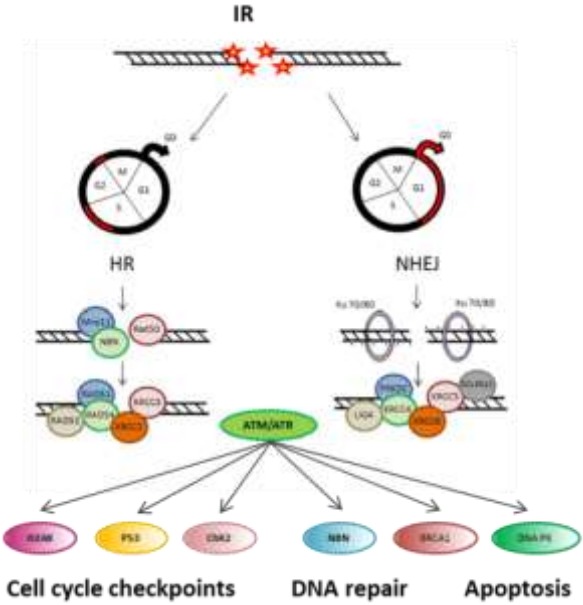

Fig. 9 Cell Cycle Control of DNA Repair [122]
Activation of HR and NHEJ repair pathways during cell cycle progression.

4. AIM

In the last years new functions of Ribosomal Proteins (RPs) have been discovered; in fact RPs not associated to eukaryotic mature ribosome show a different and specific extra-ribosomal role.

The main aim of thesis project was to identify a relationship between ribosomal stress condition and DNA damage caused by Ionizing Radiation (IR) treatment.

In particular, to verify the extra-ribosomal role of RPS19 during DNA Damage Response (DDR).

Experimental condition consisted in induce ribosomal stress through RPS19 depletion and cause DNA damage by IR exposure.

To assess thesis aims the experiments were performed in human normal primary fibroblasts MRC-5, human glioblastoma U251-MG cells which show missense point in the *p53* gene resulting in the loss of sequence-specific DNA binding and human colon cancer HCT116 cells.

5. RESULTS

5.1 RPS19 knockdown

To induce ribosomal stress condition, RPS19 was knocked-down by specific small interfering RNA (siRNA). In order to obtain the optimal reduction of RPS19 protein expression, fibroblasts, glioblastoma and colon cancer cells were transiently transfected with different concentrations of siRNA against RPS19 (iRPS19) for different times, or with a control scramble siRNA (iSCR).

The depletion of RPS19 was analyzed by western blot analysis that showed strongly protein reduction at 48 and 72 hours after transfection.

In particular, RPS19 protein level detected in fibroblasts was reduced of 50% respect to control transfected cells at 72 hours.

On the contrary, RPS19 depletion in glioblastoma cancer cells was observed 48 hours after siRNA transfection: RPS19 amount was reduced of 60% compared to iSCR cells.

Finally HCT116 cells were transfected for 24, 48 and 72 hours. Nevertheless RPS19 protein level was not reduced at 24 hours, RPS19 knockdown was observed after 48 and 72 hours after transfection. The lowest RPS19 protein amount was observed at 48 hours, indeed protein level decreased to 80% respect to iSCR cells.

In each cell line, the highest RPS19 knockdown was obtained using 15 nM of siRNA concentration. These conditions, shown in Fig. 10, set our experimental cellular condition.

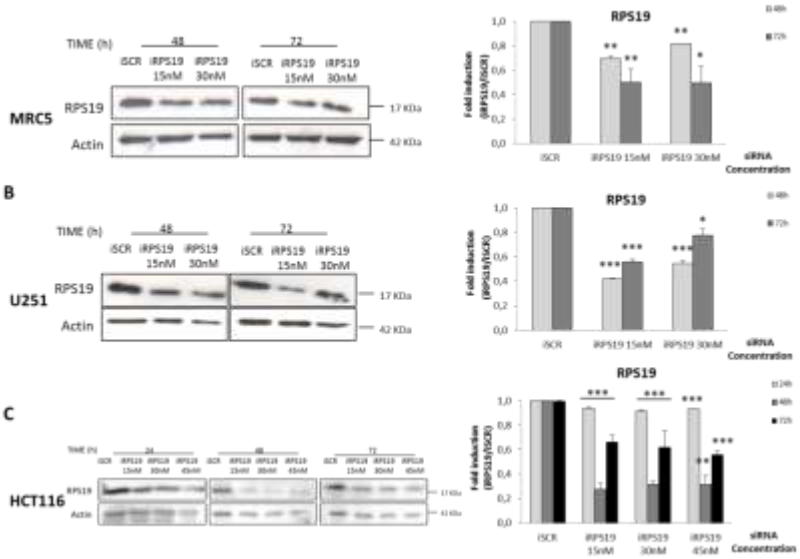

Fig. 10 RPS19 knockdown

MRC-5 (**A**), U251-MG (**B**) and HCT116 (**C**) cell lines were transfected with the indicated doses of iRPS19 or iSCR and lysed 24, 48 or 72 hours after transfection. Western blots were performed using anti RPS19 and anti Actin antibodies. Protein levels were quantified and normalized to the levels of Actin. **A-B-C** blots are representative of an experiment.

The graphs represent the RPS19 level in iRPS19 versus iSCR cells, for each experimental point.

Error bars represent standard deviation of the mean calculated from minimum of three independent experiments (*P<0.05, **P<0.01, ***P<0.001, Student's t-test)

(iSCR:control siRNA; iRPS19:transfection with siRPS19).

5.2 IR causes eEF2 iper-phosphorylation during ribosomal stress

Eukaryotic protein synthesis process is highly regulated. Literature data demonstrated that both ribosomal stress condition [16] and IR treatment [123] reduce total protein synthesis. To verify the effects of RPS19 depletion following IR-induced DNA damage on the translation process, the protein levels of ph-Ser240/244-RPS6 (p-RPS6) and of ph-Thr56-eEF2 (p-eEF2) were monitored, as described in Fig 11.

RPS19 depletion did not affect p-RPS6 level (Fig. 11 A-B-C, pRPS6, lanes 1-2, t0). Moreover data obtained in all the cell lines tested, showed that the phosphorylation of RPS6 was not affected by IR both in absence and in presence of RPS19 (Fig. 11 A-B-C, pRPS6, lanes 3-8).

According to literature data, ribosomal stress caused high phosphorylation level of eEF2 [16]. During RPS19 knockdown, eEF2 iper-phosphorylation was observed in cancer cells (Fig. 11 B-C, peEF2, lanes 1-2, t0) but not in fibroblasts (Fig. 11 A, peEF2, lanes 1-2, t0). In U251-MG and HCT116 iSCR irradiated cells, the level of p-eEF2 increased. Indeed at 24 hours, p-eEF2 was 50% higher than basal level (Fig. supplementary S1). IR treatment in ribosomal stress condition caused the iper-phosphorylation of eEF2 starting from 8 hours after induced damage, only in cancer cell lines (Fig. supplementary S1). By comparison to iRPS19 unirradiated cells, the highest phosphorylation of eEF2 was observed at 16 hours, especially in HCT116 cells (Fig. supplementary S1).

With respect to iSCR irradiated cells, p-eEF2 level of iRPS19 irradiated cells increased (Fig. 11 B-C, peEF2, lanes 3-8). In particular the highest different fold was recorded at 16 hours post-irradiation, in which p-eEF2 amount increased approximately by 50% in gliobastoma and almost of two folds in colon cancer cells. High level of p-eEF2 was observed till 24 hours, when the detected protein amount was the same of iSCR irradiated cells (Fig. 11 B-C, peEF2, lanes 3-8).

Data obtained in fibroblasts did not show changes in the p-eEF2 level after IR, neither in iSCR nor in iRPS19 cells (Fig. 11 A, peEF2, lanes 3-8).

In conclusion, IR treatment promoted early eEF2 iper-phosphorylation in cancer RPS19-depleted cells, meaning the block of elongation phase of translation.

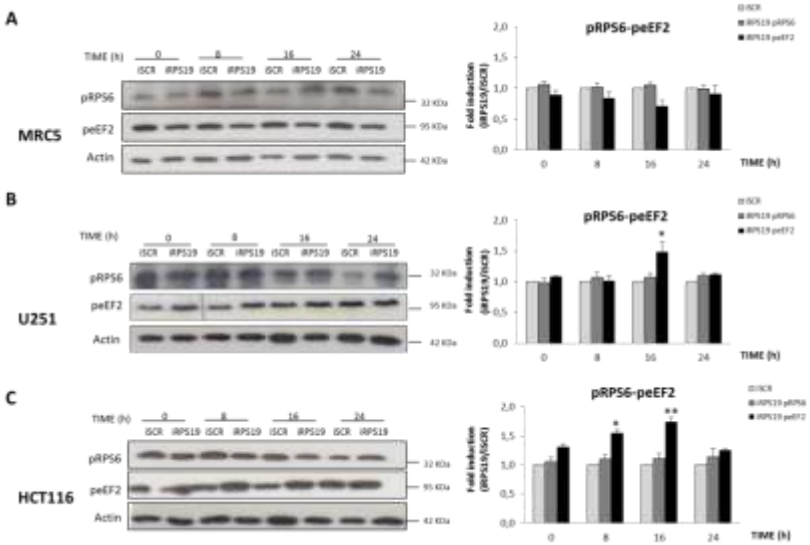

Fig. 11 Time course of p-RPS6 and p-eEF2 protein levels in iRPS19 irradiated cells

MRC-5 (**A**), U251-MG (**B**) and HCT116 (**C**) cells were irradiated with 5 Gy of X-Rays, 48 or 72 hours after transfection. Protein samples were collected and lysed 0 (unirradiated), 8, 16 or 24 hours after irradiation. Western blots were performed using anti ph-Ser240/244-RPS6 (p-RPS6), anti ph-Thr56-eEF2 (p-eEF2) anti Actin antibodies. Protein levels were quantified and normalized to the levels of Actin. **A-B-C** blots are representative of an experiment.

The graphs represent the fold induction of p-RPS6 and p-eEF2 protein levels in iRPS19 versus iSCR cells, for each experimental point.

Error bars represent standard deviation of the mean calculated from minimum of three independent experiments (*P<0.05, **P<0.01, ***P<0.001, Student's t-test)

(iSCR:control siRNA; iRPS19:transfection with siRPS19).

5.3 p53 is activated after RPS19 knockdown and IR

It has been reported that ribosomal stress induces p53 stabilization [62], therefore its total protein amount was evaluated.

Data obtained in all the cell lines analyzed showed that RPS19 depletion did not cause a strong p53 accumulation (Fig. 12 A-B-C, p53, lanes 1-2, t0), while X-Ray exposure increased p53 level both in iSCR and in RPS19-depleted cells (Fig. supplementary S2). By comparison to iRPS19 unirradiated cells, IR treatment in addition to ribosomal stress condition increased protein level starting from 8 hours and the highest amount was detected at 16 hours. In particular, p53 protein level increased by 40% in

fibroblasts, 50% in glioblastoma and 60% in colon cancer cells. p53 level was then reduced at 24 hours (Fig. supplementary S2).
With respect to iSCR irradiated cells, p53 amount was almost 50% higher at 16 hours while the increase was strongly reduced at 24 hours, since protein returned to basal level both in iSCR and in iRPS19 irradiated cells (Fig. 12 A-B-C, p53, lanes 3-8).
Nevertheless the tumor suppressor was accumulated after X-Ray exposure, iRPS19-depleted cells showed higher level of p53 than iSCR cells.
Once stabilized, the tumor suppressor is able to activate downstream factors such as p21/CDKN1A (p21).
Ribosomal stress led to p21 accumulation in all cell lines, indeed protein level recorded was almost 30% higher than in iSCR cells (Fig. 12 A-B-C, p21, lanes 1-2, t0). X-Ray treatment in control cells caused p21 stabilization, whose level was increased at 8 and 16 hours until returned to basal at 24 hours (Fig. supplementary S3). P21 protein level was also modulated in iRPS19 irradiated cells: p21 increased starting from 8 hours and high level was observed until 24 hours after induced damage (Fig. supplementary S3).
By comparison to iSCR irradiated cells, p21 level observed in iRPS19 irradiated cells increased up to a maximum of 70% in fibroblasts and 60% in cancer cells (Fig. 12 A-B-C, p21, lanes 3-8).
Data, shown in Fig. 12, indicated a higher and persistent accumulation of p21 during ribosomal stress condition.

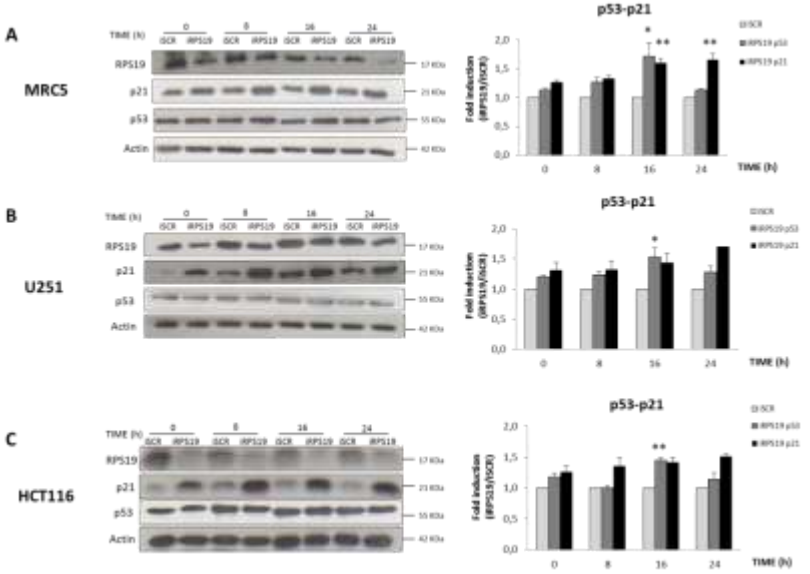

Fig. 12 p53-p21 protein levels in iRPS19 irradiated cells

MRC-5 (**A**), U251-MG (**B**) and HCT116 (**C**) cells were irradiated with 5 Gy of X-Rays, 48 or 72 hours after transfection. Protein samples were collected and lysed 0 (unirradiated), 8, 16 or 24 hours after irradiation.

Western blots were performed using anti p53, anti p21and anti Actin antibodies. Protein levels were quantified and normalized to the levels of Actin. **A-B-C** blots are representative of an experiment.

The graphs represent the fold induction of p53 and p21 protein levels in iRPS19 versus iSCR cells, for each experimental point.

Error bars represent standard deviation of the mean calculated from minimum of three independent experiments (*P<0.05, **P<0.01, ***P<0.001, Student's t-test) (iSCR:control siRNA; iRPS19:transfection with siRPS19).

To investigate about the mechanisms of p53 and p21 protein up-regulation, transcriptional analysis was performed through qRT-PCR. RPS19 knockdown did not alter p53 mRNA amount. Indeed, p53 transcriptional level was unaltered after IR treatment, both in absence and in presence of RPS19. This result was observed in each analyzed cell lines (Fig. 13 A-B-C, p53).

On the other hand ribosomal stress induced high transcriptional level of p21, which, respect to iSCR unirradiated cells, increased by three folds in MRC-5 and HCT116 cells (Fig. 13 A-C, p21, t0). In addition, qRT-PCR analysis described high quantity of endogenous mRNA also after damage:

high level of p21 mRNA was showed after IR exposure, both in iSCR and in iRPS19 irradiated cells. In particular, iSCR irradiated cells showed double amount of p21 mRNA at 6 and 20 hours; while it increased by six folds at 6 hours and eight folds at 20 hours in iRPS19 irradiated cells (Fig. 13 A-C, p21).

On the contrary, p21 transcription was never altered in glioblastoma cells. As ribosomal stress condition, also IR did not affect p21 transcription: p21 mRNA was not modulated after damage, neither in iSCR nor in iRPS19 U251-MG cells (Fig. 13 B, p21).

Transcriptional data, reported in Fig. 13 showed p21 transcriptional modulation during RPS19 depletion and IR exposure. So, IR treatment in ribosomal stress condition enhanced p21 transcription.

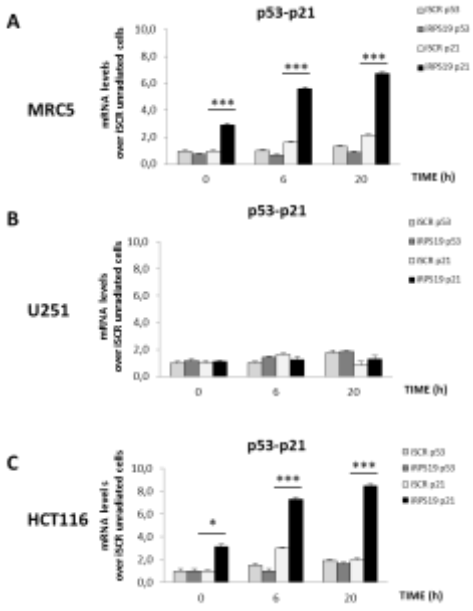

Fig.13 Transcriptional analysis of p53 and p21 mRNAs

MRC-5 (**A**), U251-MG (**B**) and HCT116 (**C**) cells were irradiated with 5 Gy of X-Rays, 48 or 72 hours after transfection. Samples were collected and lysed 0 (unirradiated), 6 and 20 hours after irradiation.

The mRNA levels of p53 and p21 were assayed by quantitative real-time PCR. Data shown are the relative amounts of specific mRNA normalized to the Actin and then to the iSCR unirradiated sample.

A-B-C graphs are representative of a minimum of three independent experiments, for each experimental point.

Error bars represent standard deviation of the mean calculated from minimum of three independent experiments (*P<0.05, **P<0.01, ***P<0.001, Student's t-test) (iSCR:control siRNA; iRPS19:transfection with siRPS19).

5.4 RPS19 depletion does not induce cells accumulation in G1 phase

The tumor suppressor p53 can block cell cycle as response to specific cellular conditions, such as ribosomal stress [47] and DNA damage [115]. Since results in Fig.12 showed that ribosomal stress alone did not cause a significant p53 activation while IR increased p53 and p21 amount, to verify whether p53 and p21 proteins modulation might in turn affect cell cycle progression, immunofluorescence BrdU assay was used to mark only cells able to entry in S phase.

RPS19 depletion in MRC-5 did not alter the number of cells in S phase (Fig. 14 A, t0), while IR treatment reduced the number of iSCR positive cells, which was further reduced in iRPS19 irradiated cells (Fig 14 A).

Also iRPS19 transfection did not reduce the percentage of HCT116 cells in S phase (Fig. 14 C, t0), which was affected by X-Rays (Fig. 14 C). Indeed, both in iSCR and in iRPS19 cells, the number was reduced approximately of 50% than in unirradiated cells. With respect to control cells, the number of HCT116 iRPS19 cells in S phase was reduced by exposure, especially 6 hours post-irradiation.

On the other hand, BrdU assay of U251-MG showed that ribosomal stress alone (Fig. 14 B, t0) and IR did not affect the percentage of glioblastoma cells in S phase, both in iSCR and in iRPS19 cells (Fig. 14 B).

In addition, FACS analysis (Fig. supplementary S4) did not reported strong alterations in cell cycle after RPS19 knockdown alone, in all cell lines.

RPS19 depletion did not cause G1 accumulation in all analyzed cell lines, while, in fibroblasts and in colon cancer cells, IR reduced the number S positive cells.

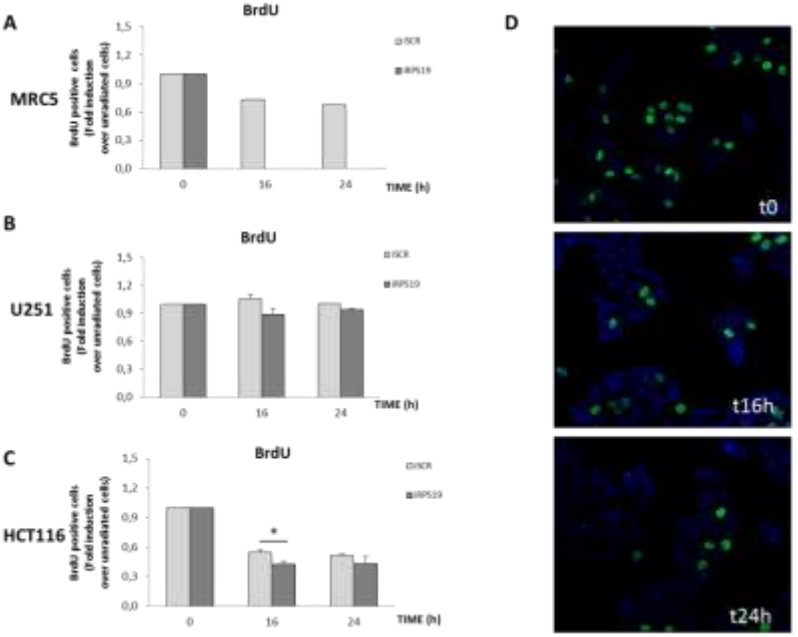

Fig. 14 Detection of cells in S phase

MRC-5 (**A**), U251-MG (**B**) and HCT116 (**C**) were irradiated cells with 5 Gy of X-Rays, 48 or 72 hours after transfection. The presence of cells in S phase was determined at 0 (unirradiated), 16 and 24 hours after irradiation, allowing cells to incorporate 45μM BrdU in the last hours before harvesting.

The graphs represent the fold induction of irradiated cells versus unirradiated cells, for each experimental point.

Error bars represent standard deviation of the mean calculated from minimum of three independent experiments (*P<0.05, **P<0.01, ***P<0.001, Student's t-test).

D: Representative pictures of cells in S phase .

DNA was counterstained with DAPI (blue) and anti-BrdU (green).

(iSCR:control siRNA; iRPS19:transfection with siRPS19).

5.5 γ-H2AX and 53BP1 recruitment is affected by ribosomal stress and IR

Damage induced to DNA leads to DSBs that can be solved through DDR pathways [89]. One of the first factor involved is H2AX which, once phosphorylated (γ-H2AX), produces foci. In order to verify whether IR treatment in ribosomal stress condition alters H2AX foci formation, the

number of γ-H2AX foci was recorded 0.5, 3 and 6 hours post-irradiation. Moreover to better discriminate foci formation, each cell lines were irradiated using 2 Gy of X-Rays.

RPS19 depletion alone did not affect γ-H2AX foci number (Fig. 15 A-B-C, t0). According to literature, IR induced γ-H2AX foci formation, which highest number was observed at 0.5 hours after exposure. In fact, in iSCR irradiated cells, the number of foci increased 6, 3 and 2 folds in fibroblasts, glioblastoma and colon cancer cells respectively. The number of foci decreased at 3 hours and was further reduced at 6 hours (Fig. supplementary S5). In iRPS19 irradiated cells, γ-H2AX activation was the same of iSCR cells. Indeed, the highest number of γ-H2AX foci was recorded at 0.5 hours and increased by 8, 4 and 2 folds in fibroblasts, glioblastoma and colon cancer cells, respect to untreated iRPS19 cells (Fig. supplementary S5). γ-H2AX foci number decreased of 50% at 3 hours and was further reduced at 6 hours after treatment (Fig. supplementary S5).

By comparison to iSCR irradiated cells, the number of foci recorded at 0.5 hours in iRPS19 cells was statistically higher, indicating that RPS19 depletion increased γ-H2AX foci formation. Moreover, the difference was strongly reduced at 3 and 6 hours (Fig. 15 A-B-C). Data indicated different activation of γ-H2AX in iRPS19 cells, especially 0.5 hours after damage.

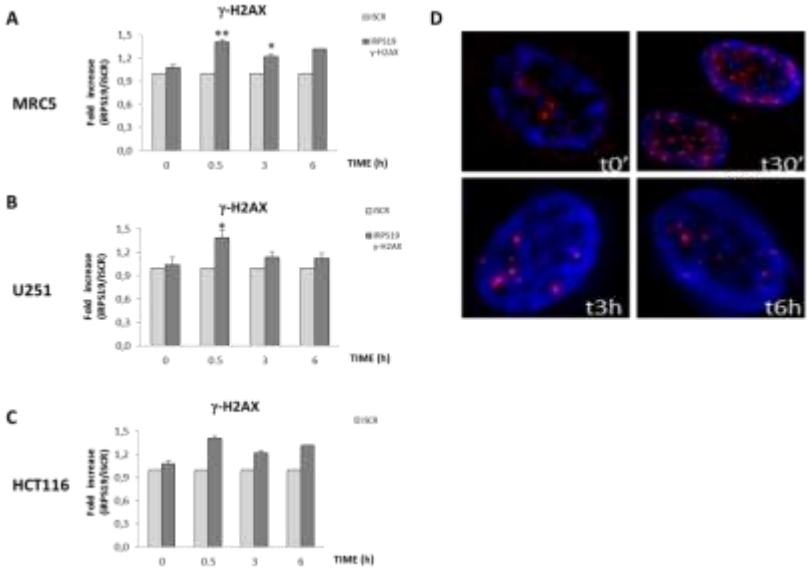

Fig. 15 γ-H2AX foci formation

MRC-5 (**A**), U251-MG (**B**) and HCT116 (**C**) were irradiated cells with 2 Gy of X-Rays, 48 or 72 hours after transfection. Number of foci was determined at 0 (unirradiated), 0.5, 3 and 6 hours after irradiation.

The graphs represent the fold induction of γ-H2AX foci in iRPS19 versus iSCR cells, for each experimental point.

Error bars represent standard deviation of the mean calculated from minimum of three independent experiments (*P<0.05, **P<0.01, ***P<0.001, Student's t-test).

D: Representative pictures of γ-H2AX foci formation after IR exposure.

DNA was counterstained with DAPI (blue) and anti-γ-H2AX (red).

(iSCR:control siRNA; iRPS19:transfection with siRPS19).

53BP1 is a sensor factor for DSBs able to colocalize with γ-H2AX in IRIF after damage [95]. For this reason, 53BP1 protein redistribution was evaluated using the conditions set for γ-H2AX marker.

RPS19 depletion alone did not affect the number of 53BP1 foci (Fig. 16 A-B-C, t0), while IR treatment induced 53BP1 accumulation. In each iSCR irradiated analyzed cell lines, the highest number of 53BP1 foci was recorded at 0.5 hours and decreased starting from 3 hours after treatment (Fig. supplementary S6). Moreover the same 53BP1 kinetic was observed in iRPS19 irradiated cells. In fact the highest number of foci, observed at 0.5 hours, decreased at 3 and 6 hours after IR (Fig. supplementary S6).

With respect to iSCR irradiated cells, IR treatment in ribosomal stress resulted in a higher foci number, mainly at 0.5 hours (Fig. 16 A-B-C).
Results, observed in fibroblasts and cancer cells, described a high 53BP1 activation in ribosomal stress condition.

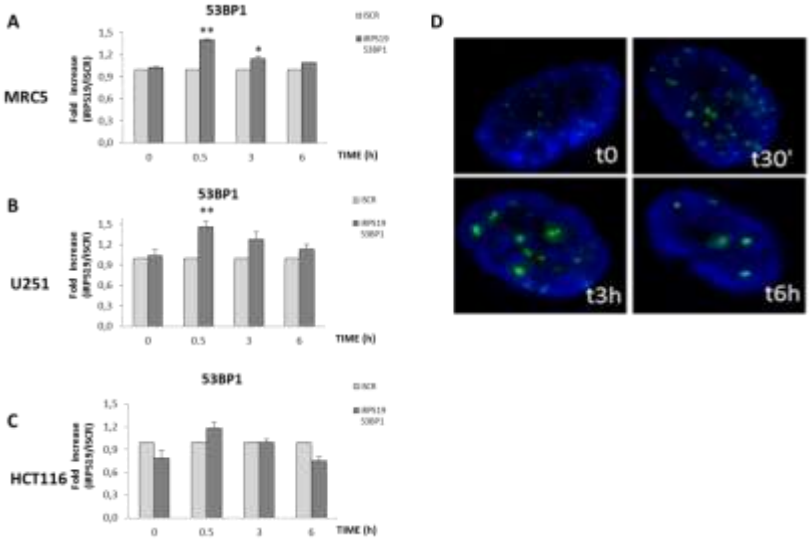

Fig. 16 53BP1 foci formation
MRC-5 (**A**), U251-MG (**B**) and HCT116 (**C**) were irradiated cells with 2 Gy of X-Rays, 48 or 72 hours after transfection. Number of foci was determined at 0 (unirradiated), 0.5, 3 and 6 hours after irradiation.
The graphs represent the fold induction of 53BP1 foci in iRPS19 versus iSCR cells, for each experimental point.
Error bars represent standard deviation of the mean calculated from minimum of three independent experiments (*P<0.05, **P<0.01, ***P<0.001, Student's t-test).
D: Representative pictures of 53BP1 foci formation after IR exposure.
DNA was counterstained with DAPI (blue) and anti-53BP1 (green).
(iSCR:control siRNA; iRPS19:transfection with siRPS19).

5.6 p-ATM activation is altered during ribosomal stress and IR

Literature data establish the centrality of ATM serine/threonine kinase in DDR pathway. DSBs lead to activation of ATM through autophosphorylation on Ser1981 site and its sequent monomerizzation [91]. Since ATM activation is directly linked to γ-H2AX and 53BP1 foci formation, the level of ph-Ser1981-ATM (p-ATM) was monitored by western blot analysis.

In all cell line analyzed, p-ATM level was not modified by RPS19 depletion (Fig. 17 A-B-C, pATM, lanes 1-2, t0), while IR rapidly activated the kinase. In iSCR irradiated cells, p-ATM level increased by 80% in MRC-5 and 60% in cancer cells at 0.5 hours after damage. Then protein level decreased progressively until return basal at 8 hours (Fig. supplementary S7). X-Ray exposure in iRPS19 cells slowed down the normal p-ATM activation.
With respect to iRPS19 unirradiated cells, p-ATM amount was doubled at 0.5 hours and further increased at 2 hours. Nevertheless, protein level decreased at 4 hours, high level was recorded until 8 hours after DNA induced damage (Fig. supplementary S7).
By comparison to iSCR irradiated cells, iRPS19 cells showed the same protein amount at 0.5 hours, but higher level of phosphorylation persisted at 2, 4 and 8 hours. The different fold, highest at 2 hours, was maintained till 8 hours after IR. Deregulation of p-ATM was observed in each RPS19-depleted cell lines (Fig. 17 A-B-C, pATM, lanes 3-10).
The amount of total protein ATM was additionally evaluated. In each analyzed cell lines, ATM level was unaltered during ribosomal stress (Fig. 17 A-B-C, ATM, lanes 1-2, t0). Similarly and according to literature data, no protein level change was observed after irradiation, in iSCR and in iRPS19-depleted cells (Fig. 17 A-B-C, ATM, lanes 3-10).
Nevertheless ATM total protein level was not affected by ribosomal stress, its activation was prolonged after IR exposure.

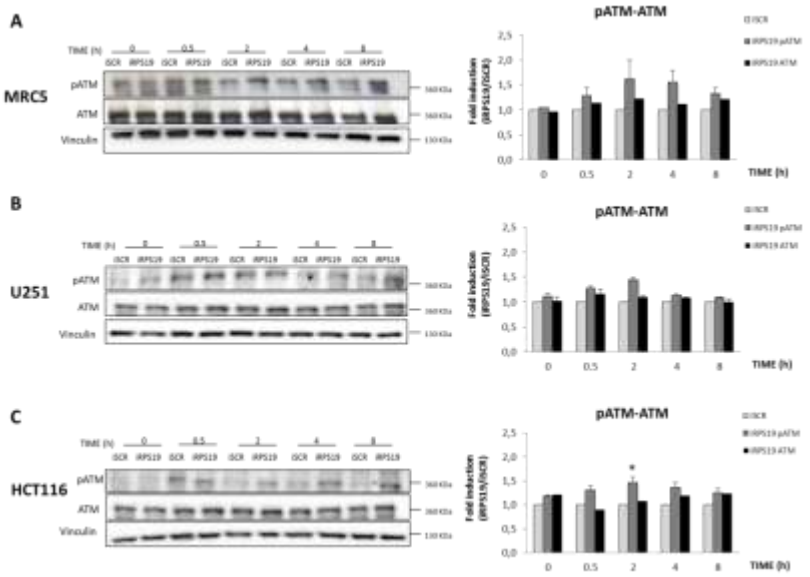

Fig. 17 Time course analysis of p-ATM and ATM proteins in iRPS19 irradiated cells
MRC-5 (**A**), U251-MG (**B**) and HCT116 (**C**) cells were irradiated with 5 Gy of X-Rays, 48 or 72 hours after transfection. Protein samples were collected and lysed 0 (unirradiated), 0.5, 2, 4 and 8 hours after irradiation. Western blots were performed using anti ph-Ser1981-ATM (p-ATM) , anti ATM and anti Vinculin antibodies. Protein levels were quantified and normalized to the levels of Vinculin. **A-B-C** blots are representative of an experiment.
The graphs represent the fold induction of p-ATM and ATM protein levels in iRPS19 versus iSCR cells, for each experimental point.
Error bars represent standard deviation of the mean calculated from minimum of three independent experiments (*P<0.05, **P<0.01, ***P<0.001, Student's t-test)
(iSCR:control siRNA; iRPS19:transfection with siRPS19).

5.7 p-CHK2 activation is altered in colon cancer cells after RPS19 depletion and IR

CHK2 can be directly activated by ATM kinase through phosphorylation on Thr68 [111]. To verify the effects of RPS19 depletion following IR-induced DNA damage on p-ATM/p-CHK2 axis, the level of ph-Thr68-CHK2 (p-CHK2) was checked.
RPS19 depletion did not affect p-CHK2 level in any cell line analyzed (Fig. 18 A-B-C, pCHK2, lanes 1-2, t0), while radio-induced damage promoted CHK2 phosphorylation. In fact, in iSCR irradiated cells, p-CHK2 protein

level was doubled at 0.5 hours and was progressively reduced at 8 hours (Fig. supplementary S8).
HCT116 iRPS19 irradiated cells showed alterations of p-CHK2 activation, as well for p-ATM. Indeed, with respect to iRPS19 unirradiated cells, Thr68 residue showed rapid activation at 0.5 hours and its level was detected till 8 hours after exposure (Fig. supplementary S8 C). The highest amount was observed at 2 hours, where an increase of 4 folds was detected (Fig. supplementary S8 C).
By comparison to HCT116 iSCR irradiated cells, iRPS19 cells showed the highest protein level at 2 hours. However, the different fold was detectable till 8 hours after IR (Fig. 18 C, pCHK2, lanes 3-10) .
Western blot results of RPS19-depleted fibroblasts and glioblastoma cells indicated different results: p-CHK2 protein level was the same for iSCR and iRPS19 irradiated cells (Fig. 18 A-B, pCHK2, lanes 3-10).
As shown in Fig. 18, p-CHK2 activation was significantly prolonged in HCT116 RPS19-depleted and irradiated cells respect to control irradiated cells.

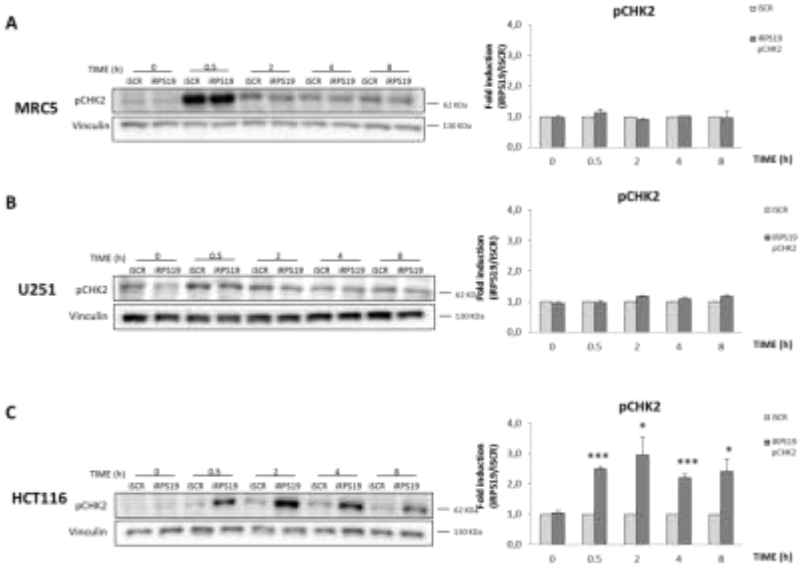

Fig. 18 Time course analysis of p-CHK2 protein in iRPS19 irradiated cells
MRC-5 (**A**), U251-MG (**B**) and HCT116 (**C**) cells were irradiated with 5 Gy of X-Rays, 48 or 72 hours after transfection. Protein samples were collected and lysed 0 (unirradiated), 0.5, 2, 4 and 8 hours after irradiation. Western blots were performed using anti ph-Thr68-CHK2 (p-

CHK2) and anti Vinculin antibodies. Protein levels were quantified and normalized to the levels of Vinculin. **A-B-C** blots are representative of an experiment.
The graphs represent the fold induction of p-CHK2 protein level in iRPS19 versus iSCR cells, for each experimental point.
Error bars represent standard deviation of the mean calculated from minimum of three independent experiments (*P<0.05, **P<0.01, ***P<0.001, Student's t-test)
(iSCR:control siRNA; iRPS19:transfection with siRPS19).

5.8 p-p53 activation is altered in glioblastoma cells after RPS19 depletion and IR

ATM activated kinase directly phosphorylates p53 on Ser15 [110]. Western blot analysis was performed to verify ph-Ser15-p53 (p-p53) alteration in iRPS19 alone or in combination with IR.
Ribosomal stress alone did not affect the phosphorylation level of p53 in each analyzed cell lines (Fig. supplementary S10 A-B-C, lanes 3-4, t0); on the contrary IR activated p-p53 only in U251-MG cell line (Fig. supplementary S10 B lanes 5-12). In fact, data about iSCR irradiated cells showed that p-p53 protein level was enhanced 4 folds at 4 hours and its amount was progressively reduced until recover to basal level at 24 hours (Fig. supplementary S9). p-p53 activation was altered in glioblastoma iRPS19 irradiated cells, as well for p-ATM activation. Indeed, p-p53 protein level enhanced 6 folds at 4 hours and it was detectable until 24 hours after IR exposure (Fig. supplementary S9).
By comparison to iSCR irradiated cells, iRPS19 irradiated cells displayed higher level of protein: at 8 hours after exposure p-p53 amount was 60% higher. A significant amount of p-p53 was recorded till 24 hours post irradiation (Fig. 19, pp53, lanes 3-10);
Data, shown in Fig. 19 displayed higher and prolonged p53 phosphorylation level in glioblastoma iRPS19 irradiated cells compared to iSCR irradiated cells. Different results were observed in fibroblasts and colon cancer cells, since IR treatment did not cause phosphorylation of p53, both in iSCR and in iRPS19 cells (Fig. supplementary S10 A, C).
As positive control, DNA damage was induce by Etoposside (VP16) treatment: colon cancer treated cells showed p53 phosphorylation (Fig. supplementary S10 C, lanes 1-2), which was no recorded in fibroblasts treated cells (Fig. supplementary S10 A, lanes 1-2). Moreover, VP16 treatment caused p53 phosphorylation in glioblastoma cells (Fig. supplementary S10 B, lanes 1-2), as well as X-Ray exposure.

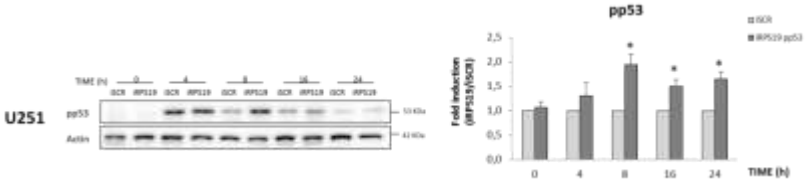

Fig. 19 Time course of p-p53 protein in iRPS19 irradiated cells

U251-MG cells were irradiated with 5 Gy of X-Rays, 48 or 72 hours after transfection. Protein samples were collected and lysed 0 (unirradiated), 4, 8, 16 and 24 hours after irradiation. Western blots were performed using anti ph-Ser15-p53 (p-p53) and anti Actin antibodies. Protein levels were quantified and normalized to the levels of Actin. Blot is representative of an experiment.

The graphs represent the fold induction of p-p53 protein level in iRPS19 versus iSCR cells, for each experimental point.

Error bars represent standard deviation of the mean calculated from minimum of three independent experiments (*P<0.05, **P<0.01, ***P<0.001, Student's t-test)
(iSCR:control siRNA; iRPS19:transfection with siRPS19).

5.9 MRN complex is not altered by ribosomal stress and IR

As described in the introduction (Cap. 3.8) the complex MRN, composed by MRE11/ RAD50/NBN proteins, is a DNA damage sensor [9].

Western blot analysis was performed to monitor MRN complex protein levels, since data seemed to indicate alterations in upstream factors.

Results showed that RPS19 knockdown alone did not modify the total amount of MRE11, RAD50 and NBN proteins (Fig. 20 A-B-C, MRE11-RAD50-NBN, lanes 1-2, t0). According to literature, IR treatment did not affect protein levels, both in absence and in presence of RPS19 (Fig. 20 A-B-C lanes 3-8).

Western blot revealed no alterations in MRN complex proteins levels after RPS19 depletion alone and in combination to X-Ray exposure.

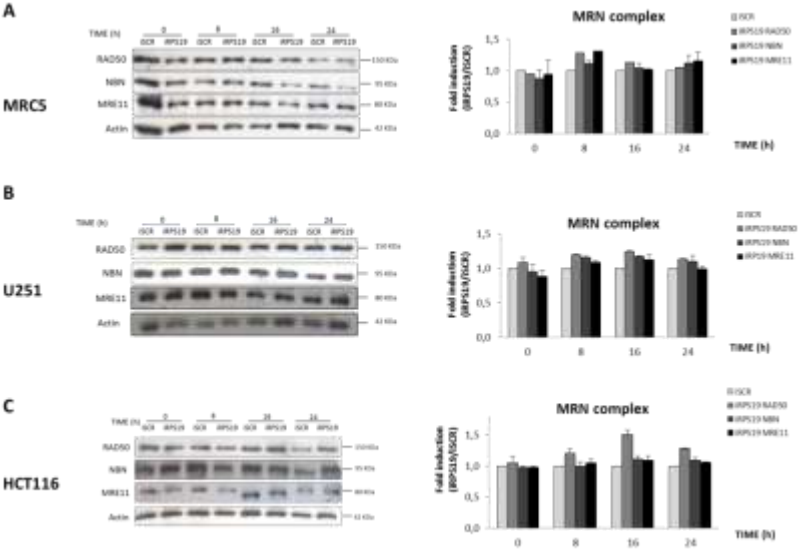

Fig.20 MRN complex protein levels in iRPS19 irradiated cells.

MRC-5 (**A**), U251-MG (**B**) and HCT116 (**C**) cells were irradiated with 5 Gy of X-Rays, 48 or 72 hours after transfection. Protein samples were collected and lysed 0 (unirradiated), 8, 16 and 24 hours after irradiation. Western blots were performed using anti RAD50, anti NBN, anti MRE11 and anti Actin antibodies. Protein levels were quantified and normalized to the levels of Actin. **A-B-C** blots are representative of an experiment.

The graphs represent the fold induction of MRN complex protein levels in iRPS19 versus iSCR cells, for each experimental point.

Error bars represent standard deviation of the mean calculated from minimum of three independent experiments (*P<0.05, **P<0.01, ***P<0.001, Student's t-test)

(iSCR:control siRNA; iRPS19:transfection with siRPS19).

As well as protein levels, ribosomal stress alone did not affect MRE11 and NBN foci formation (Fig. 21 A-B-C, t0). On the other hand, IR promoted MRE11 and NBN activation; in fact the number of foci recruited were doubled at 0.5 hours and returned to basal level at 3 hours after exposure. Such behavior in MRE11/NBN recruitment was observed both in iSCR and in iRPS19 irradiated cells (data not shown).
With respect to iSCR irradiated cells, the number of foci recorded in iRPS19 irradiated cells was not altered both at 0.5 and 3 hours after IR treatment (Fig. 21).
Results from immunofluorescence staining with specific antibodies indicated that the recruitment of MRE11 and NBN was not affected by RPS19 depletion alone and in addition to IR.

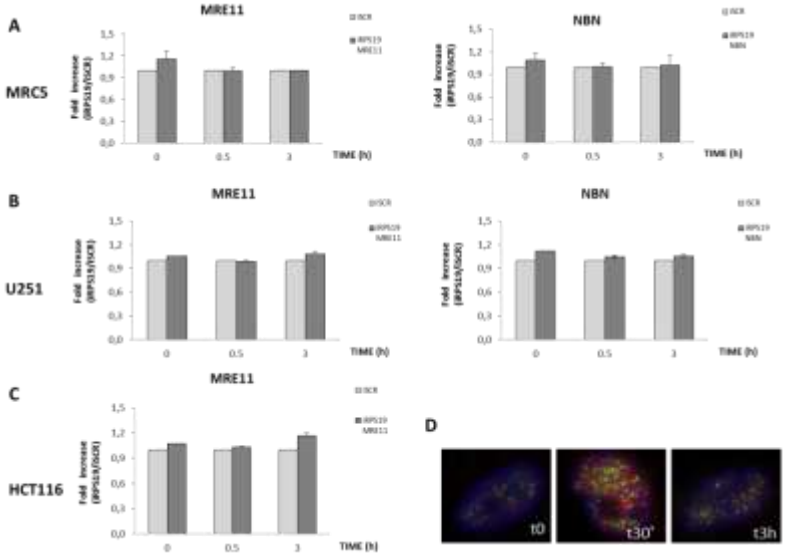

Fig. 21 Analysis of MRN complex foci formation
MRC-5 (**A**), U251-MG (**B**) and HCT116 (**C**) were irradiated cells with 5 Gy of X-Rays, 48 or 72 hours after transfection. Number of foci was determined at 0 (unirradiated), 0.5 and 3 hours after irradiation. The graphs represent the fold induction of MRE11 and NBN foci in iRPS19 versus iSCR cells, for each experimental point.
Error bars represent standard deviation of the mean calculated from minimum of three independent experiments (*P<0.05, **P<0.01, ***P<0.001, Student's t-test).
D: Representative pictures of MRE11 and NBN foci formation after IR exposure.
DNA was counterstained with DAPI (blue), anti-MRE11 (green) and anti-NBN (red).
(iSCR:control siRNA; iRPS19:transfection with siRPS19).

5.10 RAD51 protein level and foci recruitment are down-regulated during ribosomal stress and IR

RAD51 is a key factor involved in the HR pathway, responsible of strand invasion and migration to allow the correct DNA lesion repair [101].
In order to assess whether RAD51 protein level and recruitment might be affected by ribosomal stress, western blot (Fig. 22) and immunofluorescence (Fig. 24) analysis were carried out.
Data showed that RPS19 depletion alone caused RAD51 protein reduction; indeed protein amount was reduced of about 20% (Fig. 22 A-B-C, lanes 1-2, t0). X-Ray exposure did not affect RAD51 total amount in iSCR cells (Fig. supplementary S11). On the contrary, IR modulated RAD51 protein level in RPS19-depleted cells. In fact, respect to iRPS19 unirradiated cells, RAD51 amount was reduced from 8 to 24 hours, when it was recorded the lowest protein amount (Fig. supplementary S11).
RAD51 protein was strongly reduced also in comparison to iSCR irradiated cells: protein level was reduced approximately of 50% at 24 hours after exposure, in all iRPS19 cell lines (Fig. 22 A-B-C, lanes 3-8).
Results described that RAD51 was down-regulated after RPS19 depletion alone and in combination with IR; in particular the highest reduction was recorded in colon cancer cells (Fig. 22 C, lanes 3-8).

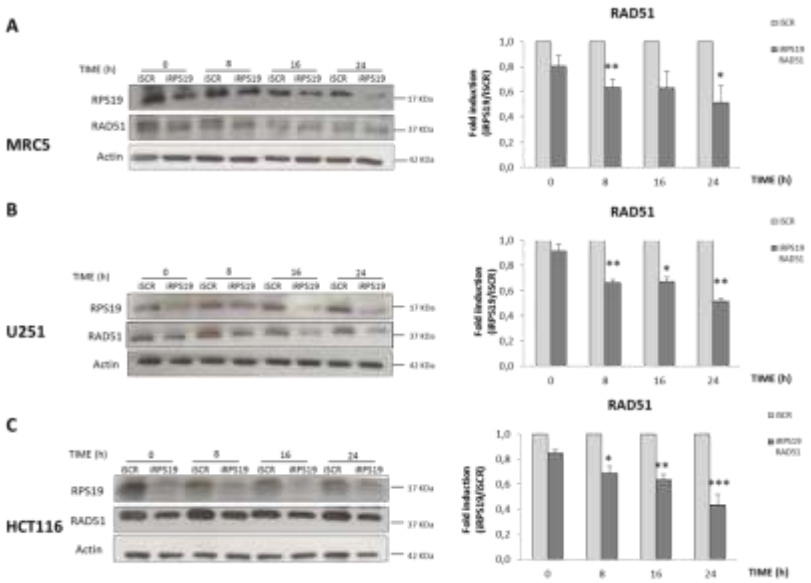

Fig. 22 RAD51 protein level in iRPS19 irradiated cells

MRC-5 (**A**), U251-MG (**B**) and HCT116 (**C**) cells were irradiated with 5 Gy of X-Rays, 48 or 72 hours after transfection. Protein samples were collected and lysed 0 (unirradiated), 8, 16 and 24 hours after irradiation. Western blots were performed using anti RAD51 and anti Actin antibodies. Protein levels were quantified and normalized to the levels of Actin. **A-B-C** blots are representative of an experiment.

The graphs represent the fold induction of RAD51 protein level in iRPS19 versus iSCR cells, for each experimental point.

Error bars represent standard deviation of the mean calculated from minimum of three independent experiments (*P<0.05, **P<0.01, ***P<0.001, Student's t-test)
(iSCR:control siRNA; iRPS19:transfection with siRPS19).

In order to investigate the mechanisms responsible of RAD51 protein down-regulation, qRT-PCR analysis was performed.

In fibroblasts and in glioblastoma cells, RPS19 depletion alone reduced RAD51 mRNA (Fig. 23 A-B, t0). In addition, mRNA level was further reduced after irradiation at 6 and 20 hours in iRPS19 cells (Fig. 23 A-B). However the reduction observed during RPS19 depletion alone and in addition to IR treatment cannot be considered statistically significant.

Moreover, data obtained in HCT116 cells showed that RAD51 transcription was not affected by IR, both in absence and in presence of RPS19 (Fig. 23 C).

Therefore, ribosomal stress condition and IR did not alter RAD51 transcription.

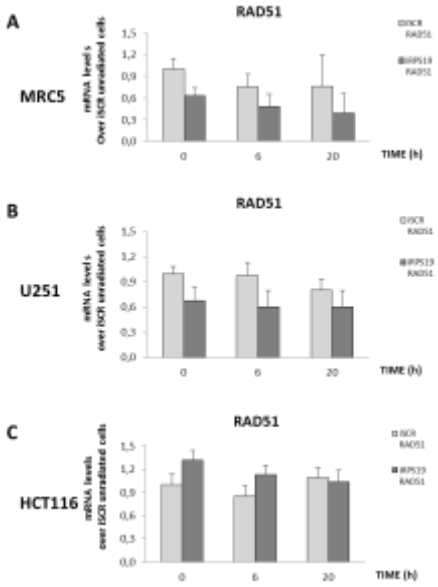

Fig.23 Transcriptional analysis of RAD51 mRNA

MRC-5 (**A**), U251-MG (**B**) and HCT116 (**C**) cells were irradiated with 5 Gy of X-Rays, 48 or 72 hours after transfection. Samples were collected and lysed 0 (unirradiated), 6 and 20 hours after irradiation.

The mRNA level of RAD51 were assayed by quantitative real-time PCR. Data shown are the relative amounts of specific mRNA normalized to the Actin and then to the iSCR unirradiated sample.

A-B-C graphs are representative of a minimum of three independent experiments, for each experimental point.

Error bars represent standard deviation of the mean calculated from minimum of three independent experiments (*P<0.05, **P<0.01, ***P<0.001, Student's t-test) (iSCR:control siRNA; iRPS19:transfection with siRPS19).

Since RAD51 needs to be recruited at sites of DNA damage to accomplish its function in HR, immunofluorescence staining of RAD51 foci was carried out after ribosomal stress condition (Fig. 24)

RPS19 depletion alone did not strongly affect RAD51 foci formation (Fig. 24 A-B-C, t0), while IR induced RAD51 activation. Indeed RAD51 foci formation started at 2 hours and the highest fold, observed at 6 hours, increased to 1.7 folds in fibroblasts, 2 folds in glioblastoma and 2.5 folds in colon cancer cells. Recovery to basal condition was observed at 24 hours (Fig. supplementary S12). IR treatment in iRPS19 cells caused correct RAD51 activation until 2 hours after damage. In fact, RPS19 knockdown affected RAD51 foci formation only at 6 hours: the number of foci recorded was similar than previous time point analyzed (Fig. supplementary S12).

By comparison to iSCR irradiated cells, RAD51 activation was deregulated by RPS19 depletion, in each cell line analyzed.

In particular, the number of foci recorded in iRPS19 irradiated cells was lower than counterpart cells and the highest different fold was observed at 6 hours after IR. Results described that RPS19 depletion impaired RAD51 foci formation (Fig. 24).

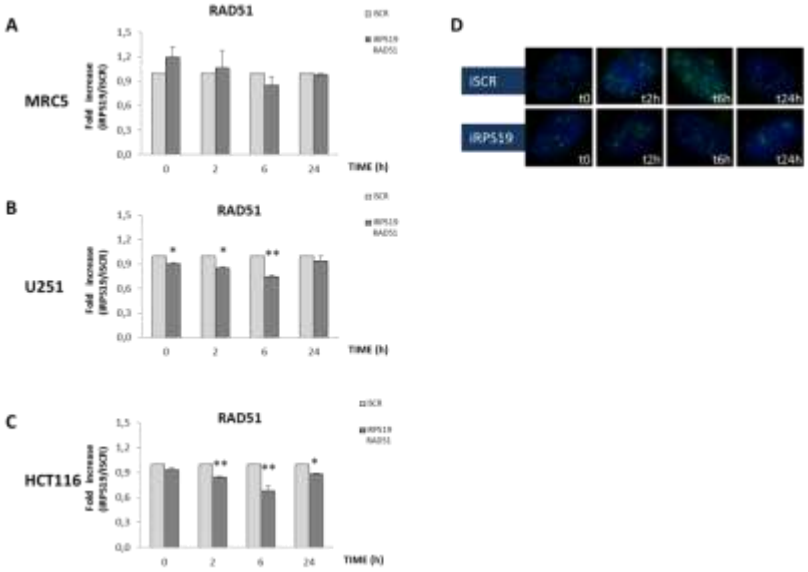

Fig. 24 Analysis of RAD51 foci formation
MRC-5 (**A**), U251-MG (**B**) and HCT116 (**C**) were irradiated cells with 5 Gy of X-Rays, 48 or 72 hours after transfection. Number of foci was determined at 0 (unirradiated), 2, 6 and 24 hours after irradiation.
The graphs represent the fold induction of RAD51 foci in iRPS19 versus iSCR cells, for each experimental point.
Error bars represent standard deviation of the mean calculated from minimum of three independent experiments (*P<0.05, **P<0.01, ***P<0.001, Student's t-test).
D: Representative pictures of RAD51 foci formation after IR exposure.
DNA was counterstained with DAPI (blue) and anti-RAD51 (green).
(iSCR:control siRNA; iRPS19:transfection with siRPS19).

Data reported in literature indicated an indirect interaction between RAD51 and RPS19. In fact RPS19 can physically interact with RAD52 [124], which it is knock to be an interactor of RAD51 [96].
Therefore, a co-immunoprecipitation assay was performed to identify a possible physical interaction between RAD51 and RPS19. However, the

result of co-IP assay carried out in HCT116 cells did not support an interaction between the two factors under investigation (Fig. 25).
Consequently, RPS19 depletion seemed not to be the mechanism responsible for the RAD51 protein level reduction (Fig. 25).

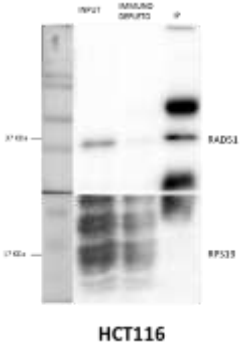

Fig.25 Analysis of RAD51-RPS19 interaction
Five hundred micrograms total protein extracts of HCT116 cells were immunoprecipitated with anti RAD51 antibody and 10 μg of total protein lysate were loaded as input. Membranes were probed with anti RAD51 and anti RPS19 antibodies

Based on the negative results of qRT-PCR and co-IP, in order to find out a possible explanation for the reduction of RAD51 in iRPS19 cells, RAD51 post-translation regulation was supposed.
Taking into account that RAD51 is a client of the molecular chaperone HSP90 (heat shock protein 90) [125], I supposed that RPS19 depletion may result in HSP90 reduction, which, in turn, affects RAD51 protein level. However, as reported in Fig. 26 (A-B-C, lanes 1-2, t0), ribosomal stress condition was not accompanied by modulation of HSP90. In addition, chaperone protein level was unaltered after IR, in iSCR as well in iRPS19 cells (Fig. 26 A-B-C, lanes 3-8).

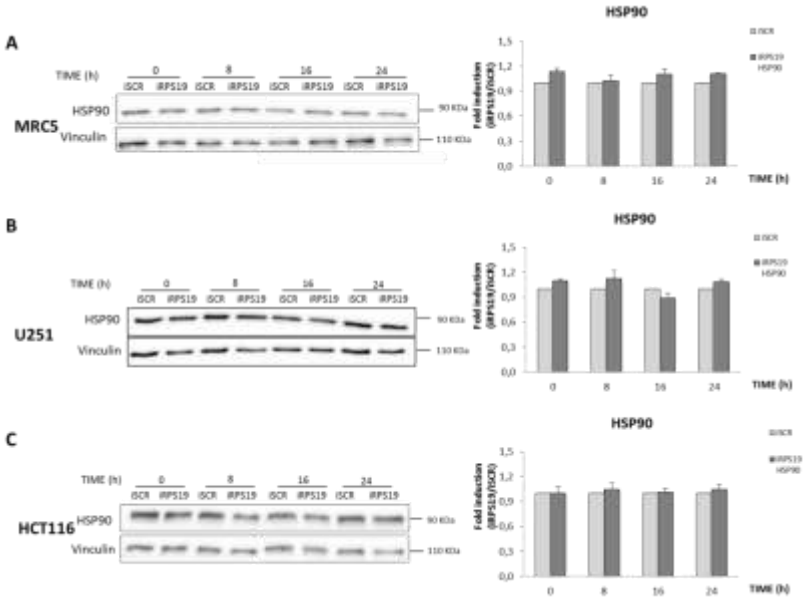

Fig. 26 HSP90 protein level in iRPS19 irradiated cells.

MRC-5 (**A**), U251-MG (**B**) and HCT116 (**C**) cells were irradiated with 5 Gy of X-Rays, 48 or 72 hours after transfection. Protein samples were collected and lysed 0 (unirradiated), 8, 16 and 24 hours after irradiation. Western blots were performed using anti HSP90 and anti Vinculin antibodies. Protein levels were quantified and normalized to the levels of Vinculin.

A-B-C blots are representative of an experiment.

The graphs represent the fold induction of HSP90 protein level in iRPS19 versus iSCR cells, for each experimental point.

Error bars represent standard deviation of the mean calculated from minimum of three independent experiments (*P<0.05, **P<0.01, ***P<0.001, Student's t-test)

(iSCR:control siRNA; iRPS19:transfection with siRPS19).

RAD51 has been identified as a client of HSP90 [125]; in addiction it is an indirect interactor of RPS19, because both RPS19 and RAD51 factors are direct interactors of RAD52 [124]. To verify whether RAD51 reduction may be linked somehow to HSP90 ATPase activity, the 17-AAG compound, a known HSP90 ATPase inhibitor [126, 127], was administered to MRC-5 cells and the level of RPS19 was evaluated.
The western blot results indicated that the level of RPS19 was unchanged after 17-AAG treatment (Fig. 27). This did not support a role for the ATPase activity of HSP90 in the RAD51 protein level reduction.

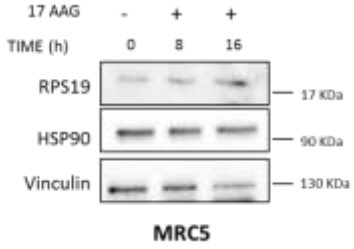

Fig.27 RPS19 protein level after HSP90 inhibition
MRC-5 cells was treated with 17AAG inhibitor. Protein samples were collected and lysed 0 (untreated), 8 and 16 hours after treatment. Western blot were performed using anti HSP90, anti RPS19 and anti Vinculin antibodies. Protein levels were quantified and normalized to the levels of Vinculn. (iSCR:control siRNA; iRPS19:transfection with siRPS19).

5.11 KU80 is not altered during ribosomal stress

HR and NHEJ pathways are activated to resolve DSBs, as response to IR-induced damage. KU80 is responsible for the assembly of the scaffold to recruit further NHEJ players [10].
Therefore, as an indirect hallmark of NHEJ impairment after ribosomal stress and IR exposure, KU80 protein was monitored by means of western blot. Results indicated that RPS19 depletion alone did not interfere with the level of KU80 expression (Fig. 28 A-B-C, lanes 1-2, t0). In a similar manner no modulation was present after IR, in iSCR and in iRPS19 cells (Fig. 28 A-B-C, lanes 3-8).
Thus, results collected in all analyzed cell lines reported no impairment of NHEJ repair pathway during ribosomal stress condition.

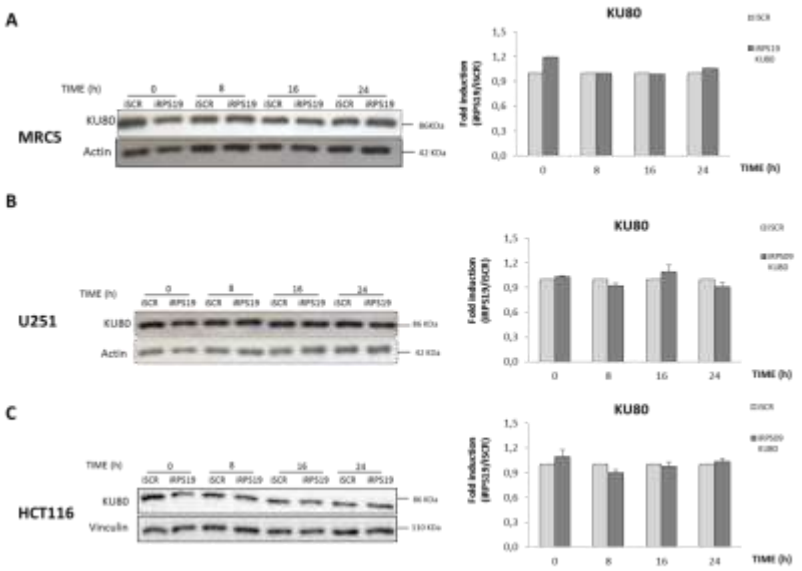

Fig. 28 KU80 protein levels in iRPS19 irradiated cells.

MRC-5 (**A**), U251-MG (**B**) and HCT116 (**C**) cells were irradiated with 5 Gy of X-Rays, 48 or 72 hours after transfection. Protein samples were collected and lysed 0 (unirradiated), 8, 16 and 24 hours after irradiation. Western blots were performed using anti KU80 and anti Vinculin antibodies. Protein levels were quantified and normalized to the levels of Vinculin.

A-**B**-**C** blots are representative of an experiment.

The graphs represent the fold induction of KU80 protein levels in iRPS19 versus iSCR cells, for each experimental point.

Error bars represent standard deviation of the mean calculated from minimum of three independent experiments (*P<0.05, **P<0.01, ***P<0.001, Student's t-test)

(iSCR:control siRNA; iRPS19:transfection with siRPS19).

6. DISCUSSION

In the last few years [56] several studies have reported about an extra-ribosomal role for Ribosomal Proteins (RPs). These functions range from development and differentiation, cell migration and invasion, cell cycle arrest and cell proliferation, to apoptosis and DNA repair. Interestingly, mutations in some RPs are causative of rare genetic disorders named "Ribosomopathies" [2] in which ribosome biogenesis is altered leading to the "Ribosomal stress" condition.

All ribosomopathies share the same clinical features, such as erythropoiesis and macrocytic anemia associated to growth retardation and development of physical abnormalities [18, 19]. One of the most studied ribosomopathia is the Diamond-Blackfan Anemia (DBA), caused by mutations mainly in the gene encoding for *RPS19* (about 25% of all reported cases) [3]. In such DBA patients, the incidence of malignancies is not very high, but is clearly above normal (acute myeloid leukemia, osteogenic sarcoma, myelodysplastic syndrome and solid tumors) [4, 7].

My study was based on the observation that an increased chromosomal sensitivity to Ionizing Radiations (IR) was found in peripheral lymphocytes of two DBA patients [6], thus indicating an extra-ribosomal function presumptive of a defective signaling/processing of Double Strand Breaks (DSBs) introduced by IR. However, it should be said that no clinical description of those patients was present in the paper done by Van Diemen et al. (1997); furthermore at that time no mutations responsible for DBA were known, since the gene responsible for DBA (1–Mb region on 19q13) was mapped by Draptchinskaia et al. (1999) [128] basing on previous studies [129-131]. More recently, also for another ribosomopathia, the Shwachman Diamond Syndrome (SDS), a defective rejoining of DSBs as measured by gamma-H2AX foci was reported [132]. Therefore, in the context of a presumptive involvement of ribosomal stress condition in the response to DNA damage, my research was addressed to clarify such relationship in normal and tumor cell lines following RPS19 knockdown.

One of the main cellular response to ribosomal stress condition is the reduction in protein synthesis caused by the block of elongation phase of translation. According to literature data, RPS19-depleted cancer cells showed the iper-phosphorylation of eEF2 factor. This could be due to an increased activation of eEF2K (Elongation Factor 2 Kinase), negative regulator of eEF2 (Elongation Factor 2), as described in myelogenous leukemia K562C and in colon cancer HCT116 RPS19-depleted cells [16].

The iper-phosphorylation of eEF2 could be due to eEF2K, activated by autophosphorylation and consequent proteasome-mediated degradation or by AMPK (AMP-activated protein Kinase) activity [133]. Moreover, a high dose of IR (10 Gy) causes iper-phosphorylation of eEF2, suggesting the presence of cellular stress which blocks the protein synthesis process [134]. While iSCR irradiated cells showed eEF2 iper-phospforylation at 24 hours after damage, in iRPS19 cells the iper-phosphorylation of eEF2 started earlier, that is from 8 hours after IR exposure, thus indicating that RPS19-depleted cells seem to be more sensitive to IR. However, a more precocious eEF2 iper-phosphorylation was expected, since RPS19 depletion alone leads to high level of p-eEF2. Thus, RPS19 knockdown in combination to moderate doses of IR (5 Gy) could promote an earlier block of protein synthesis process, as an attempt to reduce energetically expensive processes (such as translation) and activate catabolic processes [16].

One of the most interesting target of perturbations occurring to ribosomes formation is p53, a key player in the safeguard of the genome [135].

Upon ribosomal stress condition, the MDM2-p53 pathway can be regulated by different RPs [28, 47]. MDM2-p53 impairment causes the activation of tumor suppressor p53 which, in turn, activates downstream proteins, such as p21 able to block cell cycle progression at the G1/S phase transition [8]. Nevertheless the list of RPs able to bind MDM2 is still growing, no data have been yet reported about RPS19. However, erythroblasts deficient in RPS19 shows a very slight accumulation of p53 with consequent p21 increase [69], as well as primary Bone Marrow–derived $CD34^+$ [70], HCT116, LNCaP, 22RV1 and MCF7 cells [71]. Our results did not show significant differences in p53 protein level after RPS19 knockdown alone, in the three cell lines analyzed; according to protein level, also mRNA level was not modulated by RPS19 status. On the other hand, ribosomal stress condition in fibroblasts and HCT116 cells caused the increase in the basal level of p21 protein, which was mirrored also by a marked increase at mRNA level, as also reported by other authors [136]. On the contrary, iRPS19 U251-MG cells though displayed an increase in p21 protein level did not show modulation at mRNA level, possibly because of mutations in the *p53* gene (missense point mutation D3S1358) resulting in the loss of sequence-specific DNA binding. The different result on p21 expression in p53-proficient fibroblasts and HCT116 and p53-deficient U251-MG seems thus to suggest a p53-dependence for p21 modulation upon RPS19 depletion.

Concerning others RPs, Cui et al. (2013) reported that RPS26 knockdown alone led to minimal p53 protein accumulation and a slight up-regulation of

its target factors MDM2 and p21, both at protein and at mRNA levels. In addition, following RPS26 knockdown, p53 protein showed an increased half-life and was transcriptionally competent. However, after exposure to the DNA-damaging agent Doxorubicin, RPS26 was able to regulate p53 by acetylation and transactivation [85]. This suggests that RPs are able to induce p53 accumulation not only by inhibiting MDM2, but also by p53 transcriptional control.

In addition, it was reported that the depletion or mutations of specific RPs affects p53-dependent responses after induction of DNA damage. In this framework, Doxorubicin treatment in HCT116 RPS26-depleted cells did not affect p53 protein but caused p21 and MDM2 up-regulation, resulting in cell cycle arrest at G2/M [85], while, in immortalized human hepatocyte IHH cells, the topisomerase-2 inhibitor Etoposide caused rapid recruitment of p53 to the *RPS27a* gene promoter [121].

In my experiments, IR-induced damage increased p53 level which, in analyzed RPS19-depleted cells, showed higher accumulation than in iSCR-irradiated counterpart iSCR cells. However the effect observed was neither caused by up-regulation of *p53* gene expression nor by phosphorylation on Ser15, as occurs in response to IR. Thus, collected data may suggest that p53 protein amount could be stabilized by reduction in its degradation.

According to p53 accumulation, also p21 protein level increased after X-Rays, in each irradiated cell lines. Indeed, RPS19-depleted cells showed higher and longer p21 accumulation, as shown by protein level amount recorded mainly 24 hours after IR-exposure. As opposed to p53, p21 protein increased because of alteration in transcription process: high quantity of endogenous mRNA was recorded after damage, both in fibroblasts and colon cancer cells. Furthermore, p21 mRNA amount increased more in iRPS19 irradiated cells, meaning that IR treatment in ribosomal stress enhanced p21 transcription as response to cellular stress. On the other hand, in RPS19-depleted glioblastoma cells, p21 protein was accumulated as response to IR-damage independently from its transcriptional modulation, as a condition reminiscent of p21 enhanced half-life in ribosome stress condition or as consequence of in an indirect activation of p53-dependent pathway.

Nevertheless RPS19 knockdown alone resulted in p21 activation, the number of cells able to enter in S phase was not affected, as well as modulation of cell cycle. Our data were in contrast with literature, in which it was reported that RPS19 knockdown caused accumulation in G1, as in erythroid TF-1, in human $CD34^+$ haematopoietic cells [78], in erythroblasts and in chronic myelogenous leukemia K562 cells [79]; whereas RPS19

knockdown delayed G1/S-transition in mouse fetal liver cells [69] and in zebrafish [80, 81]. Moreover, DBA erythroid cells expressing low level of RPS19 arrested at the G0/G1 phase of the cell cycle [82], as well as primary fibroblasts obtained from two DBA patients which showed reduction by 50% of RPS19 and 30% of RPS24 proteins, because of mutations in RPS19 acceptor splice site (c.72-2A>C) and a RPS24 start codon (c.1A>G) [83].
As a response to IR-induced p21 accumulation, a slight impairment in the G1/S transition was recorded in fibroblasts and HCT116 cells. Otherwise G1/S transition was not affected in irradiated glioblastoma cells, an effect that could be related to their *p53* status.
Beside its role in checkpoint activation, p53 is also a factor involved in other aspects of the DNA Damage Response (DDR). IR induces DSBs that can be resolved through two main pathways: Homologous Recombination (HR) and Non Homologous End joining (NHEJ) repair pathways [86-88]. Several studies demonstrated a connection between p53 and the HR player RAD51. Notably, in my experiments, RAD51 was reduced after RPS19 knockdown. However, contrastingly to the common mechanism of RAD51 reduction reported in the literature [102], in the case of iRPS19 the modulation of the RAD51 protein was not the result of its transcriptional level. Hence, this result seems to suggest that RAD51 protein reduction was not correlated to p53 transcriptional control of *Rad51* gene promoter. Therefore, it might be hypothesized a decline of RAD51 protein stability and its consequent marked reduction, as a result of RPS19 depletion alone and in conjunction with IR-induced stress.
A possible mechanism might be as follows: RAD51 interacts with RAD52 [96] which is a known physical interactor of RPS19 [124]; hence RPS19 depletion could cause RAD52 reduction and, as indirect consequence, also the reduction in RAD51 amount. In addition, it should be pointed out that such reduction of RAD51 in iRPS19 is exacerbated by IR-exposure and this might affect the resolution of DSBs. Moreover, RAD51 foci formation was altered in iRPS19 irradiated cells; in particular the recruitment on DNA lesions started at 2 hours but did not display the same increase as detected in control-iSCR-irradiated cells. The impairment of RAD51 recruitment could be a consequence of low RAD51 protein level or could be due to p53 repression of HR; in fact p53 can physically interact with RAD51 [100] by the binding of its homo-oligomerization domain [101], thus to inhibit RAD51 foci formation. Moreover, low RAD51 protein level was not due to a direct physical interaction between RAD51 and RPS19 and it should be also excluded a link with its interactor HSP90 (heat shock protein 90) [125]. The chaperone HSP90 has a ATPase domain able to bind its molecular

target, as RAD51 [125], to inhibit ubiquitin-mediated degradation [126, 127]. However, the inhibition of ATPase activity of HSP90, caused by 17-AAG treatment, did not affect RPS19 protein level, indirect interactor of RAD51 [124]. Therefore, also post-translation modification connected with chaperone ATPase activity seems to be excluded as a possible mechanism responsible for RAD51 reduction and this issue remains to be elucidated.
RAD complex (formed by RAD51, RAD52, RAD54 and other proteins) activity is linked to MRN complex [9]. However, neither amount of MNR complex proteins nor the kinetics of NBN and MRE11 foci were affected by ribosomal stress condition alone or in conjunction with IR.
Similarly, the NHEJ repair was not affected, as described by KU80 protein, necessary for the recruitment of NHEJ players [10].
In addition to RAD51, several evidence revealed that RPs deficient cells show deregulation of DDR factors involved in HR repair, meaning that ribosomal stress condition per se causes a basal level of DNA damage. In fact, it has been reported phosphorylation of p53 Ser15 and Ser37 in RPS19 deficient human $CD34^{+}$ cells[33-35], while Danilova et al (2014) [36] described high levels of factors involved in activation of the ATR/ATM-CHK1/CHK2/p53 pathway, such as p-H2AX and p-CHK1, in RPS19 deficient zebrafish. On the contrary, in my experiments the level of mentioned HR factors were unchanged upon RPS19 depletion alone, thus not suggestive of an increased basal level of DNA damage as result of the only ribosomal stress. The difference between my work and published data could be due to cell type specificity in the response to RPS19 depletion.
In addition to data reported on RPS19 depletion alone and HR impairment, other studies include also HR response after genotoxic insult in RPs-depleted or mutated cells, as described by phosphorylation in p53 on Ser15 and Ser37, ATM Ser1981, 53BP1 Ser1778, CHK1 Ser345 and CHK2 Thr68 in RPS19-depleted zebrafish treated with Etoposside [36]. Nevertheless, no data are available on the effect of IR in a background of ribosomal stress and my data at least partly try fill this gap. Collected data indicated that RPS19 depletion affected some DDR factors (γ-H2AX, 53BP1, p-Ser1981-ATM, p-Thr68-CHK2, p-Ser15-p53, RAD51) after IR-induced damage. As mentioned in the introduction, γ-H2AX IRIF represents an early step in DDR and a recognized marker of DSBs. With respect to γ-H2AX and 53BP1 [94, 95], I found no differences between the kinetics of foci disappearance of iRPS19 and iSCR cells; however the number of both γ-H2AX and 53BP1 foci was increased at early time from irradiation, indicating that ribosomal stress rather than affecting repair might sensitize cells to radiations. One of the main kinases involved in the phosphorylation

of H2AX and responsible for the downstream activation of many HR members is the ATM kinases, which, as response to IR, is activated by rapid autophosphorylation on Ser367, Ser1893 and Ser1981 and consequent monomerizzation [91]. RPS19 knockdown led to prolonged ATM activation after IR exposure compared to control samples. Indeed iRPS19 irradiated cells showed a prolonged p-Ser1981-ATM activation, as demonstrated by protein level recorded until 8 hours after damage. Such, p-Ser1981-ATM deregulation was not simply due to an increased amount of ATM protein.
ATM kinase can directly phosphorylates CHK2 on Thr68 [111]. However, only iRPS19 colon cancer cells described alteration in p-Thr68-CHK2 protein level, which showed prolonged activation, similarly to that observed for p-Ser1981-ATM. In fact, iRPS19-HCT116 cells showed p-Thr68-CHK2 protein till 8 hours after exposure, meaning that RPS19 knockdown affected p-ATM/p-CHK2 axis in response to IR. In turn, p-Thr68-CHK2 phosphorylates p53 on Ser20 [109, 112], interfering with MDM2 binding [113]. In fact, results of HCT116-depleted cells showed that IR treatment did not induce p53 phosphorylation on Ser15, direct target of ATM kinase [110]. As positive control, DSBs induced by Etoposside treatment, promoted p-Ser15-p53 increase, meaning that IR exposure did not cause p53 phosphorylation on Ser15 in my experimental condition in this cell line. Such lack of phosphorylation was found both in iSCR and in iRPS19 cells and was in contrast to paper done by Loughery et al (2014) [137] in which was reported p-Ser15-p53 protein increase in HCT116 cells, observable mainly after 10 Gy of IR exposure. On the contrary, in iRPS19 glioblastoma irradiated cells, p-Ser15-p53 displayed higher and prolonged protein activation, as also observed for p-Ser1981-ATM, whereas no modulation of p-Thr68-CHK2 protein was detected. Data highlighted a direct link between ATM kinase and p-Ser15-p53 in iRPS19 glioblastoma cells. Moreover, it could be supposed the involvement of a third mechanism of regulation in fibroblasts. Despite p-Ser1981-ATM was deregulated, no alteration was recorded in p-Thr68-CHK2 and p-Ser15-p53 in iRPS19 irradiated fibroblasts. Thus, p53 amount could increase because of MDM2 phosphorylation on Ser395, target of ATM kinase, which in turn may possibly cause the reduction of MDM2/p53 interaction and consequently the inhibition of p53 cytoplasmic export, crucial for effective p53 degradation [114].

7. CONCLUSIONS

The aim of my project was to identify a possible extra-ribosomal function of RPS19 in response to DSBs induced by IR exposure.
Overall, I found differences in the response to IR in the cell lines used, which did not show an unique behavior, thus making the interpretation of results not easy.
The most interesting result that I found, which showed statistical robustness in all the cell lines, was related to the reduction in the HR player RAD51 after RPS19 alone and in combination to IR.
Normally, HR serves to maintain genetic stability by the accurate repair of DSBs and other DNA lesions that cannot be resolved by other repair processes. Therefore, I assume that the extra-ribosomal role of RPS19 could be to assure the correct activation of HR through RAD51 factor, to allow its correct nuclear localization and the correct functionality to resolve DNA lesions (Fig. 29). Thus, RPS19 depletion could induce not only sensitivity to IR but specially inability to resolve IR-induced DSBs. However, sensitivity to IR in my RPS19 depleted cells remain to be ascertained by means of appropriate assays, like neutral Comet assay for DSBs assessment.
In addition, inappropriate activity of the HR machinery may lead to indiscriminate recombination and consequent chromosomal aberrations.
However, many aspects in my research need to be clarified before assuming that RPS19 plays a role in DSBs response.

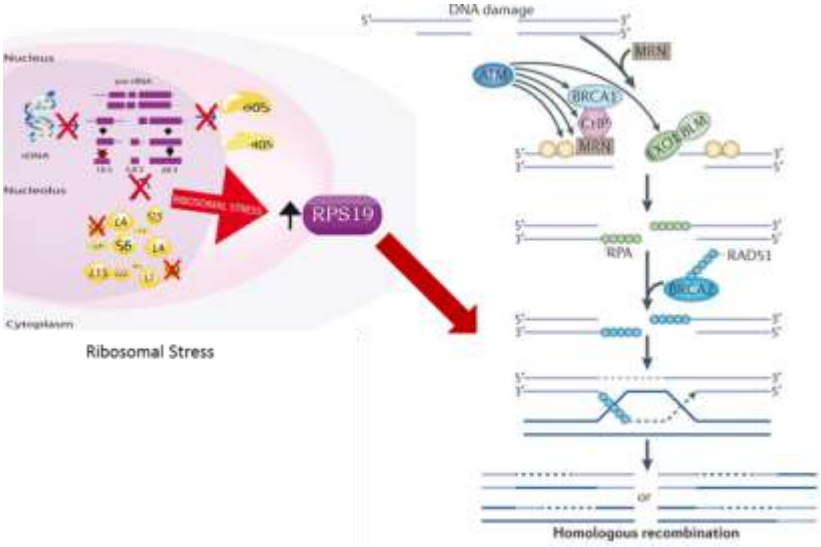

Fig. 29 Schematic representation of the extra-ribosomal role of RPS19 (modified by **[1][103])**

Ribosomal stress condition leads to free RPs, which show extra-ribosomal role. The putative role of RPS19 in the response to DNA damage caused by IR treatment could be to guarantee the correct amount of RAD51, its correct nuclear redistribution and the correct functionality to solve DNA lesions through HR. Thus, RPS19 depletion could induce not only sensitivity to IR but specially inability to solve IR-induced DSBs.

8. MATERIALS AND METHODS

8.1 Cell lines and treatment

Fetal human lung primary fibroblasts MRC-5 (ECACC, UK) were grown in MEM high glucose (Euroclone) supplemented with 10% of bovine serum, 100 U/ml of penicillin-streptomycin (25 mg/ml - 30 mg/ml), 1% of Non-Essential Amino acids and 1% of L-Glutamine.
Human glioblastoma U251-MG cells (Banca Biologica and Cell Factory, Genoa, Italy) were grown in MEM high glucose (Euroclone) supplemented with 10% of bovine serum, 100 U/ml of penicillin-streptomycin (25 mg/ml - 30 mg/ml), 1% of Non-Essential Amino acids, 1% of L-Glutamine and % of Sodium pyruvate .
Human colon cancer HCT116 cells (ISS, dept. EOMM) were grown in DMEM high glucose ultra-glutamine (Lonza) supplemented with 10% of bovine serum and 100 U/ml of penicillin-streptomycin (25 mg/ml - 30 mg/ml). Cell lines were growth at 37°C and 5% CO2 in a humidified incubator.
Bromodeoxyuridine (BrdU; Sigma) was dissolved in water and then added to cells at 45 μM final concentration for 1 hour.
Etoposside (VP16) was dissolved in DMSO and added to cells at 0.25 μM final concentration for 5 hours.
The Hsp90α inhibitor17-(Allylamino)-17-demethoxygeldanamycin (17-AAG; Sigma-Aldrich) was dissolved in DMSO and were added to cells at 1 μM final concentration for 8 and 16 hours.

8.2 siRNA transient transfection

250.000 cells were seeded in 30 mm petri dishes (around 70/80% confluence) and grown up in complete media. 8 hours later cells were transfected with specific siRNA (15 nM final concentration, Sigma-Aldirch) in Opti-MEM Reduced Serum Medium (Gibco) without antibiotics using RNAiMAX (Life Technologies), according to manufacturer's protocol. MRC-5 were incubated with siRNA for 72 hours, while cancer cells were incubated with siRNA for 48 hours. The siRNA target sequences used are follows:
sense 5'- GGGCAAAGAGAUCUGGAC -3' for human RPS19 (siRPS19)

sense- 5'- GUCUCCACGCGCAGUACAUUU -3' for scramble control siRNA (siSCR).

8.3 Ionizing radiation treatment

Cells were irradiated at room temperature with a dose of 2–5 Gy depending on the endpoint analyzed, using a MGL 300/6-D X-Rays apparatus (Gilardoni S.P.A., Mandello del Lario (LC), Italy; 250 kV, 6 mA, Cu filter) operating at a dose rate of 0.53 $Gy \cdot min^{-1}$. Cells were harvested after IR, according to the experimental plan.

8.4 Cytofluorimetric analysis of cell cycle

Transfected cells were trypsinized and washed twice with cold Phosphate Buffered Saline (PBS). Cells were fixed on ice, using cold EtOH 70% and stained with propidium iodidie (50µg/PBS 1, Sigma). Fluorescence was read in spectrofluorometer (excitation, 520 nm; analyzer, 590 nm). Experiments were repeated at least three times.

8.5 Protein extraction and western blot

To prepare protein total extracts, transfected and irradiated cells were washed in PBS and lysed in NP-40 lysis buffer (Tris HCl 20mM, NaCl 137nM, NP40 1%, EDTA 10mM, Aprotinin 1mg/ml, Leupeptin 1mg/ml, Pepstatin 1mg/ml, NaO_4V 1mM, PMSF 2mM). After 30 minutes on ice, proteins were collected by centrifugation at 13.000 rpm for 15 minutes. The supernatant was transferred into a new tube and protein concentrations were determined using the Bradford assay. Appropriate amounts were eluted in SDS-PAGE sample buffer and heated at 100°C for 5 minutes. Samples were loaded and electrophoresed. Proteins were separated on SDS polyacrylamide gels and transferred onto PVDF membrane (pore size 0.45µm, Immobilion-P). Membranes were washed in Tris Buffered Saline (TBS) 0.05% Tween-20 (TBS-T) and saturated with 5% Bovine Serum Albumin (Sigma) in TBS-T for 0.5 hours at room temperature. Membranes were incubated with the following primary antibodies at 4°C over night:

- Mouse anti p53 (DO-1) Santa Cruz Biotechnology 1:500 sc-126
- Rabbit anti p21 (M-19) Santa Cruz Biotechnology 1:200 sc-471

- Rabbit anti phospho-ATM Ser1981 (D6H9) 1:1000 Cell Signaling Technology 5883
- Mouse anti ATM (2C1) 1:200 Santa Cruz Biotechnology sc-23291
- Rabbit anti phospho-CHK2 Thr68 1:1000 Cell Signaling Technology 2661
- Mouse anti phospho-p53 Ser15 (16G8) 1:1000 Cell Signaling Technology 9286
- Rabbit anti MRE11 (H-300) 1:1000 Santa Cruz Biotechnology sc-22767
- Mouse anti RAD50 (13B3/2C6) 1:500 Santa Cruz Biotechnology sc-56209
- Mouse anti NBN (A-2) 1:1000 Santa Cruz Biotechnology sc-374168
- Rabbit anti RAD51 (y-180) 1:1000 Santa Cruz Biotechnology sc-33626
- Mouse anti HSP90 (4F10) 1:4000 Santa Cruz Biotechnology sc-69703
- Rabbit anti KU80 (C48E7) 1:2000 Cell Signaling Technology 2180
- Rabbit anti phospho-RPS6 Ser240/244 1:500 Cell Signaling Technology 5364
- Rabbit anti phospho-eEF2 Thr56 1:1000 Cell Signaling Technology 2331
- Rabbit anti RPS19 1:1000 Abcam ab187197
- Mouse anti RPS19 1:2000 Abcam ab57643
- Rabbit anti ACTIN 1:2000 Sigma-Aldrich A2066
- Mouse anti VINCULIN (VLN01) 1:4000 Sigma-Aldrich MA5-11690

After 3 washing with TBS-T for 10 minutes, membranes were incubated for 1 hour at room temperature with horseradish peroxidase-conjugated goat anti-rabbit or anti-mouse (1:10000, BioRad). After further 3 washing with TBS-T, membranes were developed using the ECL chemiluminescence detection system (BioRad). The signal were detected on films (Amersham Hyperfilm ECL, GE Healtcare) or by ImageLab 5.2.1 (BioRad). Quantification analyses were performed with ImageJ software. Actin or Vinculin were used as endogenous control for normalization. Experiments were repeated at least three times.

8.6 Immunoprecipitation

MRC-5 cells were lysed in NP-40 lysis buffer (Tris HCl 20mM, NaCl 137nM, NP40 1%, EDTA 10mM, Aprotinin 1mg/ml, Leupeptin 1mg/ml, Pepstatin 1mg/ml, NaO_4V 1mM, PMSF 2mM). 500 µg of protein were precleared by incubation with 30 µL of protein A-agarose at 4°C for 1 hour and then incubated with anti-RAD51 (1.5 µg, Santa Cruz Biotechonoly) at 4°C for 4 hours. After centrifugation at 10.000 rpm 4°C for 3 minutes, the supernatant were incubated with 30 µL of protein A-agarose at 4°C over night. After centrifugation 10.000 rpm 4°C for 3 minutes, immunoprecipitates was washed with NP-40 lysis buffer, eluted in SDS-PAGE sample buffer and then heated at 100°C for 5 minutes. The immunoprecipitates were separated on 12% SDS polyacrylamide gels, and transferred onto membrane (pore size 0.45µm, Immobilion-P). Membranes were washed in TBS- T and saturated with 5% Bovine Serum Albumin (Sigma) in TBS-T for 0.5 hours at room temperature. Membranes were thus incubated with the anti-RPS19 and anti-RAD51 primary antibodies at 4°C over night. After 3 washing with TBS-T for 10 minutes, membranes were incubated with peroxidase-conjugated goat anti-rabbit or anti-mouse Ab (1:10000, BioRad). After further 3 washing with TBS-T, membranes were developed using the ECL chemiluminescence detection system (BioRad). The signal were detected on Amersham Hyperfilm ECL, GE Healtcare) or by ImageLab 5.2.1 (BioRad). Quantification analyses were performed with ImageJ software. Actin or Vinculin were used as endogenous control for normalizations.

8.7 RNA extraction, reverse transcription and real-time PCR

To prepare RNA extracts, cells were washed in PBS and total RNAs extracted by using Trizol reagent (Invitrogen), according to manufacturer's protocol. The quality and quantity of RNA were assessed by using Nano Drop (Thermo Scientific) spectrophotometer.

500 ng of total RNA was transcribed into cDNA using SuperScript III Reverse Transcriptase (Invitrogen). cDNA, random hexamers (Invitrogen) and dNTPS (Invitrogen) were incubated at 65°C for 5 minutes. RT Buffer (Invitrogen), enzyme ssIII (Invitrogen), DTT 0.1M (Invitrogen) and RNAsi OUT (Invitrogen) were added to samples. Samples were incubated at 25°C for 5 minutes, 50° C for 45 minutes, 70°C for 15 minutes and finally at 4°C. For quantitative real-time PCR 1 ng of cDNA were added to primer forward and reverse for each analyzed gene. Transcript levels of genes were detected by Sybr Green (Ace-Q, Vazyme). Denaturation step was performed at 95°C

for 3 minutes, followed by 40 cycle of 95°C for 15 seconds and 60°C for 30 seconds for annealing and extension steps. Reactions were performed in triplicate in 96-well optical plates with Aria Mix (Agilent). Actin was used as endogenous control for normalizations. Experiments were repeated at least three times.
The sequence primers used are the follows:

- P53 sense 5'- CAGCACATGACGGAGGTTGT -3'; antisense 5'- TCATCCAAATACTCCACACGC - 3'
- P21 sense 5'- GGAAGACCATGTGGACCTGT - 3'; antisense 5' - GTCCACTGGGCCGAAGAG – 3'
- RAD51 sense 5'- GCATAAATGCCAACGATGTG - 3'; antisense 5'- GGCGTTTGGAGTGGTAGAAA - 3'
- Actin sense 5'- AGAGGGAAATCGTGCGTGAC - 3'; antisense 5'- CAATGGTGATGACCTGGCCG - 3'.

8.8 Immunoflurescence staining

For immunofluorescence staining, transfected and irradiated cells were grown on coverslip. Cells were rinsed once with cold PBS, fixed with 4% of formaldehyde at 37°C for 15 minutes and washed three times with PBS. The cells were permeabilized with 0.5% Triton X-100 in PBS at 37°C for 10 minutes and non-specific binding sites were masked with 10% Bovine Serum Albumin (Sigma) in PBS at room temperature for 1 hour. Samples were incubated for 2 hours at room temperature with following primary antibodies at 4°C over night:

- Mouse anti-phospho-Histone H2AX Ser139 (JBW301) 1:100 Millipore 05-636
- Rabbit anti-phospho-Histone H2AX Ser139 (20E3) 1:400 Cell Signaling Technology 9718
- Rabbit anti-Human 53BP1 (BP13) 1:200 NovusBio NB100-305
- Rabbit anti MRE11 (H-300) 1:1000 Santa Cruz Biotechnology sc-22767
- Mouse anti NBN (A-2) 1:1000 Santa Cruz Biotechnology sc-374168
- Rabbit anti RAD51 (y-180) 1:200 Santa Cruz Biotechnology sc-33626

After 3 washing in PBS and once in PBS 0.1% Triton X-10, cells were subsequently incubated at 37°C for 1 hour with anti-rabbit Alexa Fluor 488 or anti-mouse Alexa Fluor 564 (1:200, Invitrogen) and washed, as described

above. Cover slips were then mounted on glass slides with Vectashield mounting medium (Vector Laboratories) containing DAPI 2 µg/ml. Images were taken using a AxioImager Z2 (Zeiss) magnification 63X oil immersion objective. Quantitative analysis was carried out by counting foci in 100 cells/experimental point, in three independent experiments.

8.9 BrdU immunofluorescence staining

For BrdU immunofluorescence staining, transfected and irradiated cells were grown on coverslip. BrdU was added to cells (45µM) and incubated at 37°C for 1 hour. Cells were rinsed once with cold PBS, fixed with 4% of formaldehyde at 37°C for 15 minutes and washed three times with PBS. The cells were permeabilized with 0.5% Triton X-100 in PBS at 37°C for 10 minutes and then washed with PBS. HCL 2M was added to cells for 30 minutes at room temperature, followed by neutralization with $Na_2B_4O_7$ pH 8.5 0.1M for 15 minutes at room temperature. Cells were rinsed three times with cold PBS and non-specific binding sites were masked with 1% Bovine Serum Albumin (Sigma) in PBS for 1 hour at room temperature. Samples were incubated with anti-BrdU primary antibody (1:50; Mouse Anti Bromodeoxyuridine, Bu20a, Dako) at 4°C over night. After 3 washing in PBS and once in PBS 0.1% Triton X-10, cells were subsequently incubated for 1 hour at room temperature with anti-rabbit Alexa Fluor 488 (1:200, Invitrogen) and washed, as described above. Cover slips were then mounted on glass slides with Vectashield mounting medium for fluorescence (Vector) containing DAPI 2 µg/ml. Images were taken using AxioImager Z2 (Zeiss) magnification 40X. Quantitative analysis was carried out by counting BrdU positive cells on 500 total cells for each experimental point, in three independent experiments.

8.10 Statistical analysis

Data from at least three separate experiments are presented as means ± standard deviation (S.D.). All comparisons were calculated using Student's t-test, in which case the P values are based on a two-way ANOVA analysis. Differences with a <0.05 P-value are considered significant.
(*$P<0.05$, **$P<0.01$, ***$P<0.001$, Student's t-test).

9. REFERENCES

1. Caldarola, S., et al., *Synthesis and function of ribosomal proteins--fading models and new perspectives.* FEBS J, 2009. 276(12): p. 3199-210.
2. Freed, E.F., et al., *When ribosomes go bad: diseases of ribosome biogenesis.* Mol Biosyst, 2010. 6(3): p. 481-93.
3. Ball, S., *Diamond Blackfan anemia.* Hematology Am Soc Hematol Educ Program, 2011. 2011: p. 487-91.
4. Lipton, J.M. and S.R. Ellis, *Diamond-Blackfan anemia: diagnosis, treatment, and molecular pathogenesis.* Hematol Oncol Clin North Am, 2009. 23(2): p. 261-82.
5. Flygare, J. and S. Karlsson, *Diamond-Blackfan anemia: erythropoiesis lost in translation.* Blood, 2007. 109(8): p. 3152-4.
6. van Diemen, P.C., et al., *X-ray-sensitivity of lymphocytes of aplastic- and Diamond-Blackfan-anemia patients as detected by conventional cytogenetic and chromosome painting techniques.* Mutat Res, 1997. 373(2): p. 225-35.
7. Delaporta, P., et al., *Clinical phenotype and genetic analysis of RPS19, RPL5, and RPL11 genes in Greek patients with Diamond Blackfan Anemia.* Pediatr Blood Cancer, 2014. 61(12): p. 2249-55.
8. Quin, J.E., et al., *Targeting the nucleolus for cancer intervention.* Biochim Biophys Acta, 2014. 1842(6): p. 802-16.
9. Sancar, A., et al., *Molecular mechanisms of mammalian DNA repair and the DNA damage checkpoints.* Annu Rev Biochem, 2004. 73: p. 39-85.
10. Vignard, J., G. Mirey, and B. Salles, *Ionizing-radiation induced DNA double-strand breaks: a direct and indirect lighting up.* Radiother Oncol, 2013. 108(3): p. 362-9.
11. Grummt, I., *Regulation of mammalian ribosomal gene transcription by RNA polymerase I.* Prog Nucleic Acid Res Mol Biol, 1999. 62: p. 109-54.
12. Hahn, S., *Structure and mechanism of the RNA polymerase II transcription machinery.* Nat Struct Mol Biol, 2004. 11(5): p. 394-403.
13. Willis, I.M., *RNA polymerase III. Genes, factors and transcriptional specificity.* Eur J Biochem, 1993. 212(1): p. 1-11.
14. Fatica, A. and D. Tollervey, *Making ribosomes.* Curr Opin Cell Biol, 2002. 14(3): p. 313-8.
15. Zinzalla, V., et al., *Activation of mTORC2 by association with the ribosome.* Cell, 2011. 144(5): p. 757-68.
16. Gismondi, A., et al., *Ribosomal stress activates eEF2K-eEF2 pathway causing translation elongation inhibition and recruitment of terminal oligopyrimidine (TOP) mRNAs on polysomes.* Nucleic Acids Res, 2014. 42(20): p. 12668-80.
17. Nobukini, T. and G. Thomas, *The mTOR/S6K signalling pathway: the role of the TSC1/2 tumour suppressor complex and the proto-oncogene Rheb.* Novartis Found Symp, 2004. 262: p. 148-54; discussion 154-9, 265-8.
18. Narla, A. and B.L. Ebert, *Ribosomopathies: human disorders of ribosome dysfunction.* Blood, 2010. 115(16): p. 3196-205.
19. Shenoy, N., et al., *Alterations in the ribosomal machinery in cancer and hematologic disorders.* J Hematol Oncol, 2012. 5: p. 32.
20. Idol, R.A., et al., *Cells depleted for RPS19, a protein associated with Diamond Blackfan Anemia, show defects in 18S ribosomal RNA synthesis and small ribosomal subunit production.* Blood Cells Mol Dis, 2007. 39(1): p. 35-43.
21. Danilova, N. and H.T. Gazda, *Ribosomopathies: how a common root can cause a tree of pathologies.* Dis Model Mech, 2015. 8(9): p. 1013-26.

22. Cmejla, R., et al., *Ribosomal protein S17 gene (RPS17) is mutated in Diamond-Blackfan anemia.* Hum Mutat, 2007. 28(12): p. 1178-82.
23. Choesmel, V., et al., *Mutation of ribosomal protein RPS24 in Diamond-Blackfan anemia results in a ribosome biogenesis disorder.* Hum Mol Genet, 2008. 17(9): p. 1253-63.
24. Boria, I., et al., *A new database for ribosomal protein genes which are mutated in Diamond-Blackfan Anemia.* Hum Mutat, 2008. 29(11): p. E263-70.
25. Zhou, X., et al., *Ribosomal proteins: functions beyond the ribosome.* J Mol Cell Biol, 2015. 7(2): p. 92-104.
26. de Las Heras-Rubio, A., et al., *Ribosomal proteins as novel players in tumorigenesis.* Cancer Metastasis Rev, 2014. 33(1): p. 115-41.
27. Takada, H. and A. Kurisaki, *Emerging roles of nucleolar and ribosomal proteins in cancer, development, and aging.* Cell Mol Life Sci, 2015. 72(21): p. 4015-25.
28. Wang, W., et al., *Ribosomal proteins and human diseases: pathogenesis, molecular mechanisms, and therapeutic implications.* Med Res Rev, 2015. 35(2): p. 225-85.
29. Xu, X., X. Xiong, and Y. Sun, *The role of ribosomal proteins in the regulation of cell proliferation, tumorigenesis, and genomic integrity.* Sci China Life Sci, 2016. 59(7): p. 656-72.
30. Wool, I.G., *Extraribosomal functions of ribosomal proteins.* Trends Biochem Sci, 1996. 21(5): p. 164-5.
31. Yadavilli, S., et al., *Ribosomal protein S3: A multi-functional protein that interacts with both p53 and MDM2 through its KH domain.* DNA Repair (Amst), 2009. 8(10): p. 1215-24.
32. Esposito, D., et al., *Human rpL3 plays a crucial role in cell response to nucleolar stress induced by 5-FU and L-OHP.* Oncotarget, 2014. 5(22): p. 11737-51.
33. Ashcroft, M., Y. Taya, and K.H. Vousden, *Stress signals utilize multiple pathways to stabilize p53.* Mol Cell Biol, 2000. 20(9): p. 3224-33.
34. Vousden, K.H. and D.P. Lane, *p53 in health and disease.* Nat Rev Mol Cell Biol, 2007. 8(4): p. 275-83.
35. Levine, A.J. and M. Oren, *The first 30 years of p53: growing ever more complex.* Nat Rev Cancer, 2009. 9(10): p. 749-58.
36. Danilova, N., et al., *The role of the DNA damage response in zebrafish and cellular models of Diamond Blackfan anemia.* Dis Model Mech, 2014. 7(7): p. 895-905.
37. Bermejo, R., M.S. Lai, and M. Foiani, *Preventing replication stress to maintain genome stability: resolving conflicts between replication and transcription.* Mol Cell, 2012. 45(6): p. 710-8.
38. Li, X. and J.L. Manley, *New talents for an old acquaintance: the SR protein splicing factor ASF/SF2 functions in the maintenance of genome stability.* Cell Cycle, 2005. 4(12): p. 1706-8.
39. Hastak, K., et al., *DNA synthesis from unbalanced nucleotide pools causes limited DNA damage that triggers ATR-CHK1-dependent p53 activation.* Proc Natl Acad Sci U S A, 2008. 105(17): p. 6314-9.
40. Bester, A.C., et al., *Nucleotide deficiency promotes genomic instability in early stages of cancer development.* Cell, 2011. 145(3): p. 435-46.
41. Mannava, S., et al., *Depletion of deoxyribonucleotide pools is an endogenous source of DNA damage in cells undergoing oncogene-induced senescence.* Am J Pathol, 2013. 182(1): p. 142-51.
42. Jang, C.Y., H.D. Kim, and J. Kim, *Ribosomal protein S3 interacts with TRADD to induce apoptosis through caspase dependent JNK activation.* Biochem Biophys Res Commun, 2012. 421(3): p. 474-8.

43. Khanna, N., et al., *S29 ribosomal protein induces apoptosis in H520 cells and sensitizes them to chemotherapy.* Biochem Biophys Res Commun, 2003. 304(1): p. 26-35.
44. Jeon, Y.J., et al., *Ribosomal protein S6 is a selective mediator of TRAIL-apoptotic signaling.* Oncogene, 2008. 27(31): p. 4344-52.
45. Russo, A., et al., *Human rpL3 induces G(1)/S arrest or apoptosis by modulating p21 (waf1/cip1) levels in a p53-independent manner.* Cell Cycle, 2013. 12(1): p. 76-87.
46. Shi, Y., et al., *Ribosomal proteins S13 and L23 promote multidrug resistance in gastric cancer cells by suppressing drug-induced apoptosis.* Exp Cell Res, 2004. 296(2): p. 337-46.
47. Warner, J.R. and K.B. McIntosh, *How common are extraribosomal functions of ribosomal proteins?* Mol Cell, 2009. 34(1): p. 3-11.
48. Duan, J., et al., *Knockdown of ribosomal protein S7 causes developmental abnormalities via p53 dependent and independent pathways in zebrafish.* Int J Biochem Cell Biol, 2011. 43(8): p. 1218-27.
49. Matsson, H., et al., *Targeted disruption of the ribosomal protein S19 gene is lethal prior to implantation.* Mol Cell Biol, 2004. 24(9): p. 4032-7.
50. Anderson, S.J., et al., *Ablation of ribosomal protein L22 selectively impairs alphabeta T cell development by activation of a p53-dependent checkpoint.* Immunity, 2007. 26(6): p. 759-72.
51. Oristian, D.S., et al., *Ribosomal protein L29/HIP deficiency delays osteogenesis and increases fragility of adult bone in mice.* J Orthop Res, 2009. 27(1): p. 28-35.
52. Lindstrom, M.S. and M. Nister, *Silencing of ribosomal protein S9 elicits a multitude of cellular responses inhibiting the growth of cancer cells subsequent to p53 activation.* PLoS One, 2010. 5(3): p. e9578.
53. Matragkou, C.N., et al., *The potential role of ribosomal protein S5 on cell cycle arrest and initiation of murine erythroleukemia cell differentiation.* J Cell Biochem, 2008. 104(4): p. 1477-90.
54. McDonald, J.M., et al., *Elevated phospho-S6 expression is associated with metastasis in adenocarcinoma of the lung.* Clin Cancer Res, 2008. 14(23): p. 7832-7.
55. Wang, H., et al., *Overexpression of ribosomal protein L15 is associated with cell proliferation in gastric cancer.* BMC Cancer, 2006. 6: p. 91.
56. Neumann, F. and U. Krawinkel, *Constitutive expression of human ribosomal protein L7 arrests the cell cycle in G1 and induces apoptosis in Jurkat T-lymphoma cells.* Exp Cell Res, 1997. 230(2): p. 252-61.
57. Zhang, D., et al., *Aggregation of Ribosomal Protein S6 at Nucleolus Is Cell Cycle-Controlled and Its Function in Pre-rRNA Processing Is Phosphorylation Dependent.* J Cell Biochem, 2016. 117(7): p. 1649-57.
58. Iadevaia, V., et al., *PIM1 kinase is destabilized by ribosomal stress causing inhibition of cell cycle progression.* Oncogene, 2010. 29(40): p. 5490-9.
59. Rubbi, C.P. and J. Milner, *Disruption of the nucleolus mediates stabilization of p53 in response to DNA damage and other stresses.* EMBO J, 2003. 22(22): p. 6068-77.
60. Toledo, F. and G.M. Wahl, *Regulating the p53 pathway: in vitro hypotheses, in vivo veritas.* Nat Rev Cancer, 2006. 6(12): p. 909-23.
61. Nag, S., et al., *The MDM2-p53 pathway revisited.* J Biomed Res, 2013. 27(4): p. 254-71.
62. Miliani de Marval, P.L. and Y. Zhang, *The RP-Mdm2-p53 pathway and tumorigenesis.* Oncotarget, 2011. 2(3): p. 234-8.

63. Kubbutat, M.H., S.N. Jones, and K.H. Vousden, *Regulation of p53 stability by Mdm2*. Nature, 1997. 387(6630): p. 299-303.
64. Zhang, Y., et al., *Ribosomal protein L11 negatively regulates oncoprotein MDM2 and mediates a p53-dependent ribosomal-stress checkpoint pathway*. Mol Cell Biol, 2003. 23(23): p. 8902-12.
65. Dai, M.S., et al., *Ribosomal protein L23 activates p53 by inhibiting MDM2 function in response to ribosomal perturbation but not to translation inhibition.* Mol Cell Biol, 2004. 24(17): p. 7654-68.
66. Dai, M.S. and H. Lu, *Inhibition of MDM2-mediated p53 ubiquitination and degradation by ribosomal protein L5*. J Biol Chem, 2004. 279(43): p. 44475-82.
67. Chen, D., et al., *Ribosomal protein S7 as a novel modulator of p53-MDM2 interaction: binding to MDM2, stabilization of p53 protein, and activation of p53 function.* Oncogene, 2007. 26(35): p. 5029-37.
68. Takagi, M., et al., *Regulation of p53 translation and induction after DNA damage by ribosomal protein L26 and nucleolin.* Cell, 2005. 123(1): p. 49-63.
69. Sieff, C.A., et al., *Pathogenesis of the erythroid failure in Diamond Blackfan anaemia.* Br J Haematol, 2010. 148(4): p. 611-22.
70. Dutt, S., et al., *Haploinsufficiency for ribosomal protein genes causes selective activation of p53 in human erythroid progenitor cells.* Blood, 2011. 117(9): p. 2567-76.
71. Sagar, V., et al., *PIM1 destabilization activates a p53-dependent response to ribosomal stress in cancer cells.* Oncotarget, 2016. 7(17): p. 23837-49.
72. Chakraborty, A., T. Uechi, and N. Kenmochi, *Guarding the 'translation apparatus': defective ribosome biogenesis and the p53 signaling pathway*. Wiley Interdiscip Rev RNA, 2011. 2(4): p. 507-22.
73. Dai, M.S., X.X. Sun, and H. Lu, *Ribosomal protein L11 associates with c-Myc at 5 S rRNA and tRNA genes and regulates their expression.* J Biol Chem, 2010. 285(17): p. 12587-94.
74. Gao, M., et al., *Ribosomal protein S7 regulates arsenite-induced GADD45alpha expression by attenuating MDM2-mediated GADD45alpha ubiquitination and degradation*. Nucleic Acids Res, 2013. 41(10): p. 5210-22.
75. Daniely, Y., D.D. Dimitrova, and J.A. Borowiec, *Stress-dependent nucleolin mobilization mediated by p53-nucleolin complex formation.* Mol Cell Biol, 2002. 22(16): p. 6014-22.
76. Colombo, E., et al., *Nucleophosmin regulates the stability and transcriptional activity of p53*. Nat Cell Biol, 2002. 4(7): p. 529-33.
77. Ma, H. and T. Pederson, *Depletion of the nucleolar protein nucleostemin causes G1 cell cycle arrest via the p53 pathway*. Mol Biol Cell, 2007. 18(7): p. 2630-5.
78. Flygare, J., et al., *Deficiency of ribosomal protein S19 in CD34+ cells generated by siRNA blocks erythroid development and mimics defects seen in Diamond-Blackfan anemia*. Blood, 2005. 105(12): p. 4627-34.
79. Kuramitsu, M., et al., *Deficient RPS19 protein production induces cell cycle arrest in erythroid progenitor cells.* Br J Haematol, 2008. 140(3): p. 348-59.
80. Uechi, T., et al., *Deficiency of ribosomal protein S19 during early embryogenesis leads to reduction of erythrocytes in a zebrafish model of Diamond-Blackfan anemia*. Hum Mol Genet, 2008. 17(20): p. 3204-11.
81. Danilova, N., K.M. Sakamoto, and S. Lin, *Ribosomal protein S19 deficiency in zebrafish leads to developmental abnormalities and defective erythropoiesis through activation of p53 protein family*. Blood, 2008. 112(13): p. 5228-37.

82. Devlin, E.E., et al., *A transgenic mouse model demonstrates a dominant negative effect of a point mutation in the RPS19 gene associated with Diamond-Blackfan anemia*. Blood, 2010. 116(15): p. 2826-35.
83. Badhai, J., et al., *Ribosomal protein S19 and S24 insufficiency cause distinct cell cycle defects in Diamond-Blackfan anemia*. Biochim Biophys Acta, 2009. 1792(10): p. 1036-42.
84. Yao, Y., et al., *Down-regulation of ribosomal protein S15A inhibits proliferation of human glioblastoma cells in vivo and in vitro via AKT pathway.* Tumour Biol, 2016. 37(4): p. 4979-90.
85. Cui, D., et al., *The ribosomal protein S26 regulates p53 activity in response to DNA damage*. Oncogene, 2014. 33(17): p. 2225-35.
86. International Atomic Energy Agency, V., *Biological Dosimetry: Chromosomal Aberration Analysis for Dose Assessment.* . Technical Reports n.260.
87. Goodhead, D.T., J. Thacker, and R. Cox, *Weiss Lecture. Effects of radiations of different qualities on cells: molecular mechanisms of damage and repair.* Int J Radiat Biol, 1993. 63(5): p. 543-56.
88. Pfeiffer, P., et al., *DNA lesions and repair*. Mutat Res, 1996. 366(2): p. 69-80.
89. Ohnishi, T., E. Mori, and A. Takahashi, *DNA double-strand breaks: their production, recognition, and repair in eukaryotes.* Mutat Res, 2009. 669(1-2): p. 8-12.
90. Blanpain, C., et al., *DNA-damage response in tissue-specific and cancer stem cells.* Cell Stem Cell, 2011. 8(1): p. 16-29.
91. Bakkenist, C.J. and M.B. Kastan, *DNA damage activates ATM through intermolecular autophosphorylation and dimer dissociation*. Nature, 2003. 421(6922): p. 499-506.
92. Lavin, M.F., *ATM and the Mre11 complex combine to recognize and signal DNA double-strand breaks.* Oncogene, 2007. 26(56): p. 7749-58.
93. Lee, J.H. and T.T. Paull, *Activation and regulation of ATM kinase activity in response to DNA double-strand breaks.* Oncogene, 2007. 26(56): p. 7741-8.
94. Paull, T.T., et al., *A critical role for histone H2AX in recruitment of repair factors to nuclear foci after DNA damage.* Curr Biol, 2000. 10(15): p. 886-95.
95. Rappold, I., et al., *Tumor suppressor p53 binding protein 1 (53BP1) is involved in DNA damage-signaling pathways.* J Cell Biol, 2001. 153(3): p. 613-20.
96. Kagawa, W., et al., *Homologous pairing promoted by the human Rad52 protein.* J Biol Chem, 2001. 276(37): p. 35201-8.
97. New, J.H., et al., *Rad52 protein stimulates DNA strand exchange by Rad51 and replication protein A.* Nature, 1998. 391(6665): p. 407-10.
98. Park, M.S., et al., *Physical interaction between human RAD52 and RPA is required for homologous recombination in mammalian cells.* J Biol Chem, 1996. 271(31): p. 18996-9000.
99. Eggler, A.L., R.B. Inman, and M.M. Cox, *The Rad51-dependent pairing of long DNA substrates is stabilized by replication protein A.* J Biol Chem, 2002. 277(42): p. 39280-8.
100. Linke, S.P., et al., *p53 interacts with hRAD51 and hRAD54, and directly modulates homologous recombination.* Cancer Res, 2003. 63(10): p. 2596-605.
101. Henning, W. and H.W. Sturzbecher, *Homologous recombination and cell cycle checkpoints: Rad51 in tumour progression and therapy resistance.* Toxicology, 2003. 193(1-2): p. 91-109.
102. Arias-Lopez, C., et al., *p53 modulates homologous recombination by transcriptional regulation of the RAD51 gene.* EMBO Rep, 2006. 7(2): p. 219-24.

103. Chowdhury, D., Y.E. Choi, and M.E. Brault, *Charity begins at home: non-coding RNA functions in DNA repair.* Nat Rev Mol Cell Biol, 2013. 14(3): p. 181-9.
104. Meek, K., *New targets to translate DNA-PK signals.* Cell Cycle, 2009. 8(23): p. 3809.
105. Mladenov, E., et al., *DNA double-strand break repair as determinant of cellular radiosensitivity to killing and target in radiation therapy.* Front Oncol, 2013. 3: p. 113.
106. Leber, R., et al., *The XRCC4 gene product is a target for and interacts with the DNA-dependent protein kinase.* J Biol Chem, 1998. 273(3): p. 1794-801.
107. Yano, K., et al., *Molecular mechanism of protein assembly on DNA double-strand breaks in the non-homologous end-joining pathway.* J Radiat Res, 2009. 50(2): p. 97-108.
108. Moshous, D., et al., *Artemis, a novel DNA double-strand break repair/V(D)J recombination protein, is mutated in human severe combined immune deficiency.* Cell, 2001. 105(2): p. 177-86.
109. Shieh, S.Y., et al., *The human homologs of checkpoint kinases Chk1 and Cds1 (Chk2) phosphorylate p53 at multiple DNA damage-inducible sites.* Genes Dev, 2000. 14(3): p. 289-300.
110. Banin, S., et al., *Enhanced phosphorylation of p53 by ATM in response to DNA damage.* Science, 1998. 281(5383): p. 1674-7.
111. Matsuoka, S., et al., *Ataxia telangiectasia-mutated phosphorylates Chk2 in vivo and in vitro.* Proc Natl Acad Sci U S A, 2000. 97(19): p. 10389-94.
112. Hirao, A., et al., *DNA damage-induced activation of p53 by the checkpoint kinase Chk2.* Science, 2000. 287(5459): p. 1824-7.
113. Chehab, N.H., et al., *Chk2/hCds1 functions as a DNA damage checkpoint in G(1) by stabilizing p53.* Genes Dev, 2000. 14(3): p. 278-88.
114. Maya, R., et al., *ATM-dependent phosphorylation of Mdm2 on serine 395: role in p53 activation by DNA damage.* Genes Dev, 2001. 15(9): p. 1067-77.
115. Molinari, M., *Cell cycle checkpoints and their inactivation in human cancer.* Cell Prolif, 2000. 33(5): p. 261-74.
116. Falck, J., et al., *The ATM-Chk2-Cdc25A checkpoint pathway guards against radioresistant DNA synthesis.* Nature, 2001. 410(6830): p. 842-7.
117. Esashi, F., et al., *CDK-dependent phosphorylation of BRCA2 as a regulatory mechanism for recombinational repair.* Nature, 2005. 434(7033): p. 598-604.
118. Iliakis, G., *Backup pathways of NHEJ in cells of higher eukaryotes: cell cycle dependence.* Radiother Oncol, 2009. 92(3): p. 310-5.
119. Llanos, S. and M. Serrano, *Depletion of ribosomal protein L37 occurs in response to DNA damage and activates p53 through the L11/MDM2 pathway.* Cell Cycle, 2010. 9(19): p. 4005-12.
120. Hegde, V., et al., *DNA repair efficiency in transgenic mice over expressing ribosomal protein S3.* Mutat Res, 2009. 666(1-2): p. 16-22.
121. Nosrati, N., N.R. Kapoor, and V. Kumar, *DNA damage stress induces the expression of ribosomal protein S27a gene in a p53-dependent manner.* Gene, 2015. 559(1): p. 44-51.
122. Minafra, L., Bravatà, V., *Cell and molecular response to IORT treatment.* Transl Cancer Res 2014. 3(1): p. 32-47.
123. Braunstein, S., et al., *Regulation of protein synthesis by ionizing radiation.* Mol Cell Biol, 2009. 29(21): p. 5645-56.

124. Du, Y., et al., *Streamline proteomic approach for characterizing protein-protein interaction network in a RAD52 protein complex.* J Proteome Res, 2009. 8(5): p. 2211-7.
125. Yao, Q., B. Weigel, and J. Kersey, *Synergism between etoposide and 17-AAG in leukemia cells: critical roles for Hsp90, FLT3, topoisomerase II, Chk1, and Rad51.* Clin Cancer Res, 2007. 13(5): p. 1591-600.
126. Banerji, U., et al., *Phase I pharmacokinetic and pharmacodynamic study of 17-allylamino, 17-demethoxygeldanamycin in patients with advanced malignancies.* J Clin Oncol, 2005. 23(18): p. 4152-61.
127. Jhaveri, K. and S. Modi, *HSP90 inhibitors for cancer therapy and overcoming drug resistance.* Adv Pharmacol, 2012. 65: p. 471-517.
128. Draptchinskaia, N., et al., *The gene encoding ribosomal protein S19 is mutated in Diamond-Blackfan anaemia.* Nat Genet, 1999. 21(2): p. 169-75.
129. Gustavsson, P., et al., *Diamond-Blackfan anaemia in a girl with a de novo balanced reciprocal X;19 translocation.* J Med Genet, 1997. 34(9): p. 779-82.
130. Gustavsson, P., et al., *Diamond-Blackfan anaemia: genetic homogeneity for a gene on chromosome 19q13 restricted to 1.8 Mb.* Nat Genet, 1997. 16(4): p. 368-71.
131. Gustavsson, P., et al., *Identification of microdeletions spanning the Diamond-Blackfan anemia locus on 19q13 and evidence for genetic heterogeneity.* Am J Hum Genet, 1998. 63(5): p. 1388-95.
132. Morini, J., et al., *Radiosensitivity in lymphoblastoid cell lines derived from Shwachman-Diamond syndrome patients.* Radiat Prot Dosimetry, 2015. 166(1-4): p. 95-100.
133. Flore Kruiswijk, L.Y., Roberto Magliozzi, Teck Yew Lo, Ratna Lim, Renske Bolder, Shabaz Mohammed, Christopher G. Proud, Albert J. R. Heck, Michele Pagano, and Daniele Guardavaccaro, *Coupled activation-degradation of eEF2K regulates protein synthesis in response to genotoxic stress.* Sci Signal, 2013. 5(227).
134. Lu, X., et al., *Radiation-induced changes in gene expression involve recruitment of existing messenger RNAs to and away from polysomes.* Cancer Res, 2006. 66(2): p. 1052-61.
135. Lane, D.P., *Cancer. p53, guardian of the genome.* Nature, 1992. 358(6381): p. 15-6.
136. Abella, N., et al., *Nucleolar disruption ensures nuclear accumulation of p21 upon DNA damage.* Traffic, 2010. 11(6): p. 743-55.
137. Loughery, J., et al., *Critical role for p53-serine 15 phosphorylation in stimulating transactivation at p53-responsive promoters.* Nucleic Acids Res, 2014. 42(12): p. 7666-80.

10. SUPPLEMENTARY MATERIALS

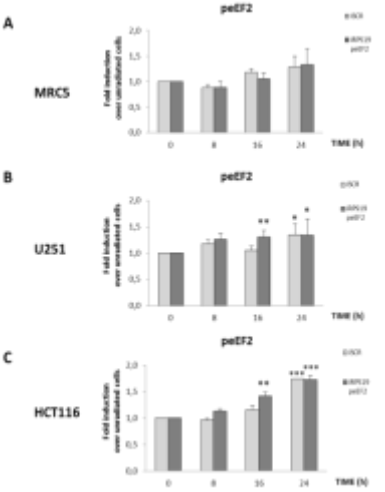

Fig. supplementary S1: p-eEF2 protein level after X-Rays
MRC-5 (**A**), U251-MG (**B**) and HCT116 (**C**) cells were irradiated with 5 Gy of X-Rays, 48 or 72 hours after transfection. Protein samples were collected and lysed 0 (unirradiated), 8, 16 or 24 hours after irradiation. Western blot were performed using anti ph-Thr56-eEF2 (p-eEF2) and anti Actin antibodies. Protein levels were quantified and normalized to the levels of Actin. The graphs represent the fold induction of p-eEF2 protein level after IR exposure versus unirradiated cells. Error bars represent standard deviation of the mean calculated from minimum of three independent experiments. Statistical analysis describes the fold induction of irradiated cells versus unradiated cells (*P<0.05, **P<0.01, ***P<0.001, Student's t-test). (iSCR:control siRNA; iRPS19:transfection with siRPS19).

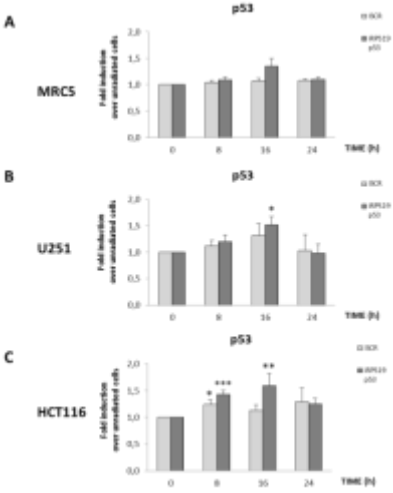

Fig. supplementary S2: p53 protein level after X-Rays
MRC-5 (**A**), U251-MG (**B**) and HCT116 (**C**) cells were irradiated with 5 Gy of X-Rays, 48 or 72 hours after transfection. Protein samples were collected and lysed 0 (unirradiated), 8, 16 or 24 hours after irradiation. Western blot were performed using anti p53 and anti Actin antibodies. Protein levels were quantified and normalized to the levels of Actin. The graphs represent the fold induction of p53 protein level after IR exposure versus unirradiated cells. Error bars represent standard deviation of the mean calculated from minimum of three independent experiments.
Statistical analysis describes the fold induction of irradiated cells versus unradiated cells (*P<0.05, **P<0.01, ***P<0.001, Student's t-test).
(iSCR:control siRNA; iRPS19:transfection with siRPS19).

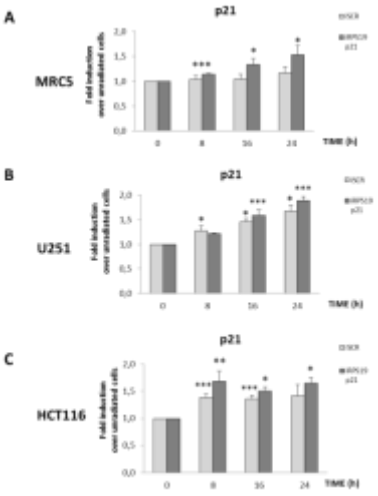

Fig. supplementary S3: p21 protein level after X-Rays

MRC-5 (**A**), U251-MG (**B**) and HCT116 (**C**) cells were irradiated with 5 Gy of X-Rays, 48 or 72 hours after transfection. Protein samples were collected and lysed 0 (unirradiated), 8, 16 or 24 hours after irradiation. Western blot were performed using anti p21 and anti Actin antibodies. Protein levels were quantified and normalized to the levels of Actin. The graphs represent the fold induction of p21 protein level after IR exposure versus unirradiated cells. Error bars represent standard deviation of the mean calculated from minimum of three independent experiments.

Statistical analysis describes the fold induction of irradiated cells versus unradiated cells (*P<0.05, **P<0.01, ***P<0.001, Student's t-test). (iSCR:control siRNA; iRPS19:transfection with siRPS19).

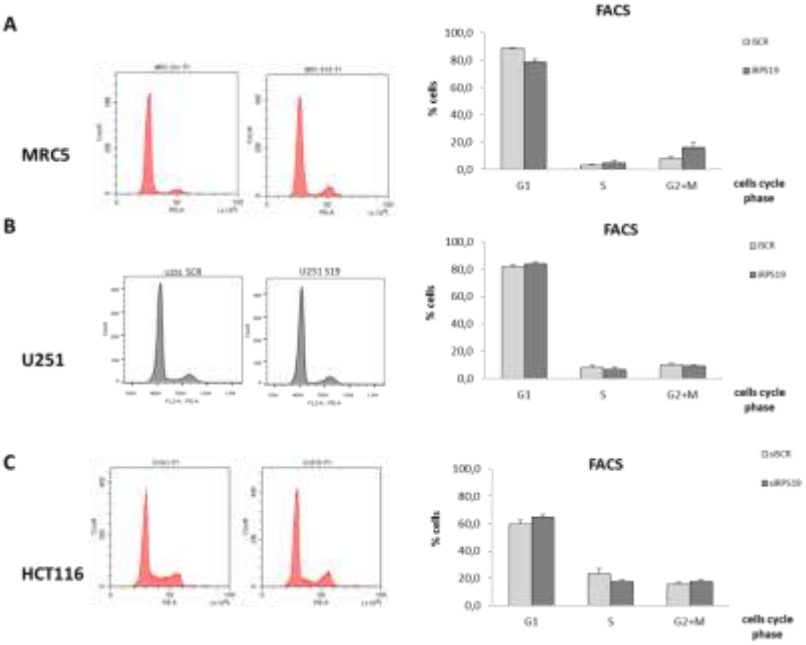

Fig. supplementary S4 FACS analysis

MRC-5 (**A**), U251-MG (**B**) and HCT116 (**C**) were fixed and stained with PI solution, 48 or 72 hours after transfection. Cell cycle analysis was carried out by cytofluorimetric analysis.

A-**B**-**C** are representative cell cycle profile.

The graphs represent cells distribution. Error bars represent standard deviation of the mean calculated from minimum of three independent experiments (*P<0.05, **P<0.01, ***P<0.001, Student's t-test). (iSCR:control siRNA; iRPS19:transfection with siRPS19).

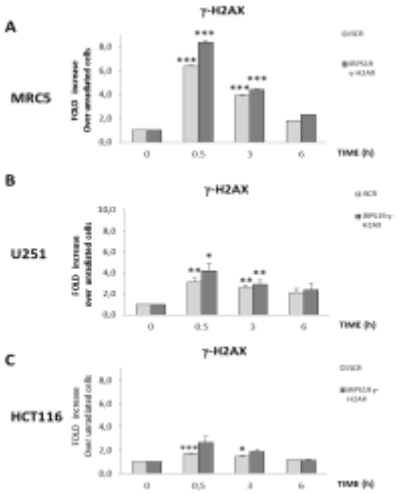

Fig. supplementary S5: γ-H2AX foci formation

MRC-5 (**A**), U251-MG (**B**) and HCT116 (**C**) were irradiated cells with 2 Gy of X-Rays, 48 or 72 hours after transfection. Number of foci was determined at 0 (unirradiated), 0.5, 3 and 6 hours after irradiation.

The graphs represent the fold induction of γ-H2AX foci of irradiated cells versus unirradiated cells. Error bars represent standard deviation of the mean calculated from minimum of three independent experiments.

Statistical analysis describes the fold induction of irradiated cells versus unradiated cells (*P<0.05, **P<0.01, ***P<0.001, Student's t-test).

(iSCR:control siRNA; iRPS19:transfection with siRPS19).

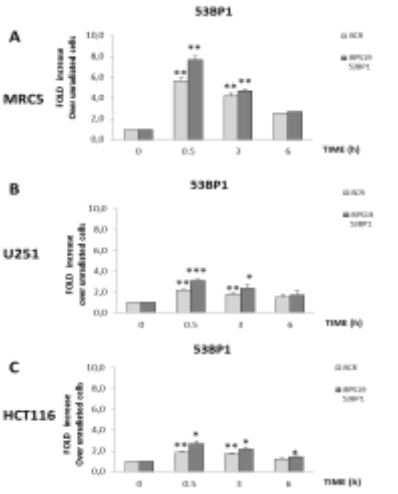

Fig. supplementary S6: 53BP1 foci formation

MRC-5 (**A**), U251-MG (**B**) and HCT116 (**C**) were irradiated cells with 2 Gy of X-Rays, 48 or 72 hours after transfection. Number of foci was determined at 0 (unirradiated), 0.5, 3 and 6 hours after irradiation.

The graphs represent the fold induction of 53BP1 foci of irradiated cells versus unirradiated cells. Error bars represent standard deviation of the mean calculated from minimum of three independent experiments.

Statistical analysis describes the fold induction of irradiated cells versus unradiated cells (*P<0.05, **P<0.01, ***P<0.001, Student's t-test).

(iSCR:control siRNA; iRPS19:transfection with siRPS19).

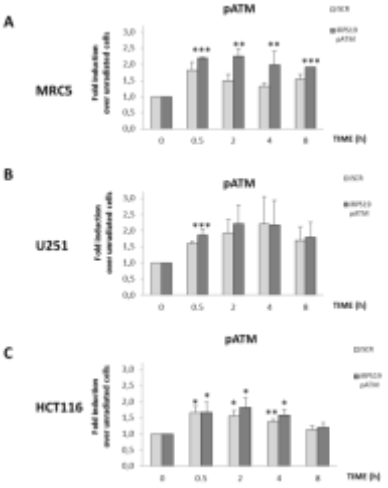

Fig. supplementary S7: p-ATM protein level after X-Rays

MRC-5 (**A)**, U251-MG (**B**) and HCT116 (**C**) cells were irradiated with 5 Gy of X-Rays, 48 or 72 hours after transfection. Protein samples were collected and lysed 0 (unirradiated), 0.5, 2, 4 and 8 hours after irradiation. Western blot were performed using anti ph-Ser1981-ATM (p-ATM) and anti Vinculin antibodies. Protein levels were quantified and normalized to the levels of Vinculin. The graphs represent the fold induction of p-ATM protein level after IR exposure versus unirradiated cells. Error bars represent standard deviation of the mean calculated from minimum of three independent experiments.

Statistical analysis describes the fold induction of irradiated cells versus unradiated cells (*P<0.05, **P<0.01, ***P<0.001, Student's t-test).

(iSCR:control siRNA; iRPS19:transfection with siRPS19).

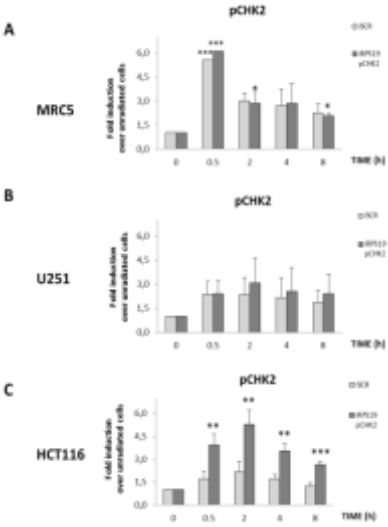

Fig. supplementary S8: p-CHK2 protein level after X-Rays

MRC-5 (**A**), U251-MG (**B**) and HCT116 (**C**) cells were irradiated with 5 Gy of X-Rays, 48 or 72 hours after transfection. Protein samples were collected and lysed 0 (unirradiated), 0.5, 2, 4 and 8 hours after irradiation. Western blot were performed using anti ph-Thr86-CHK2 (p-CHK2) and anti Vinculin antibodies. Protein levels were quantified and normalized to the levels of Vinculin. The graphs represent the fold induction of p-CHK2 protein level after IR exposure versus unirradiated cells. Error bars represent standard deviation of the mean calculated from minimum of three independent experiments.

Statistical analysis describes the induction of irradiated cells versus unradiated cells (*P<0.05, **P<0.01, ***P<0.001, Student's t-test).

(iSCR:control siRNA; iRPS19:transfection with siRPS19).

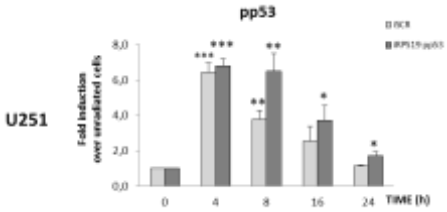

Fig. supplementary S9: p-p53 protein level in U251-MG after X-Rays

U251-MG cells were irradiated with 5 Gy of X-Rays 48 hours after transfection. Protein samples were collected and lysed 0 (unirradiated), 4, 8, 16 and 24 hours after irradiation. Western blot were performed using anti ph-Ser15-p53 (p-p53) and anti Actin antibodies. Protein levels were quantified and normalized to the levels of Actin. The graphs represent the fold induction of p-p53 protein level after IR exposure versus unirradiated cells. Error bars represent standard deviation of the mean calculated from minimum of three independent experiments.

Statistical analysis describes the fold induction of irradiated cells versus unradiated cells (*P<0.05, **P<0.01, ***P<0.001, Student's t-test).

(iSCR:control siRNA; iRPS19:transfection with siRPS19).

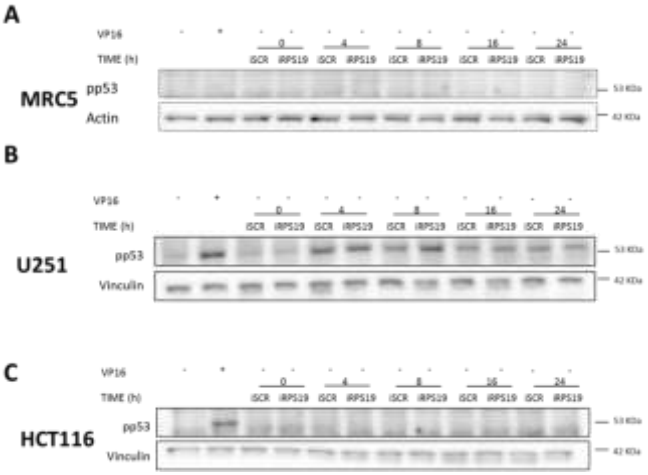

Fig. supplementary S10: p-p53 protein level in MRC-5 and HCT116 after X-Rays

MRC-5 (**A**), U251-MG (**B**) and HCT116 (**C**) cells were irradiated with 5 Gy of X-Rays, 48 or 72 hours after transfection. Protein samples were collected and lysed after VP16 treatment (+) or 0 (unirradiated), 4, 8, 16 and 24 hours after irradiation or Western blots were performed using anti ph-Ser15-p53 (p-p53) and anti Vinculin antibodies. Protein levels were quantified and normalized to the levels of Vinculin. Blots are representative of an experiment.(iSCR:control siRNA; iRPS19:transfection with siRPS19).

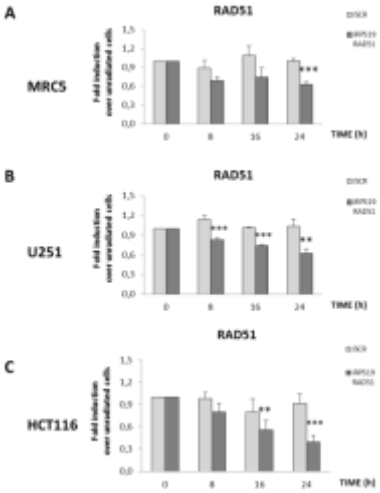

Fig. supplementary S11: RAD51 protein level after X-Rays

MRC-5 (**A**), U251-MG (**B**) and HCT116 (**C**) cells were irradiated with 5 Gy of X-Rays, 48 or 72 hours after transfection. Protein samples were collected and lysed 0 (unirradiated), 8, 16 and 24 hours after irradiation. Western blot were performed using anti RAD51 and anti Actin antibodies. Protein levels were quantified and normalized to the levels of Actin. The graphs represent the fold induction of RAD51 protein level after IR exposure versus unirradiated cells. Error bars represent standard deviation of the mean calculated from minimum of three independent experiments.

Statistical analysis describes the induction of irradiated cells versus unradiated cells (*P<0.05, **P<0.01, ***P<0.001, Student's t-test).

(iSCR:control siRNA; iRPS19:transfection with siRPS19).

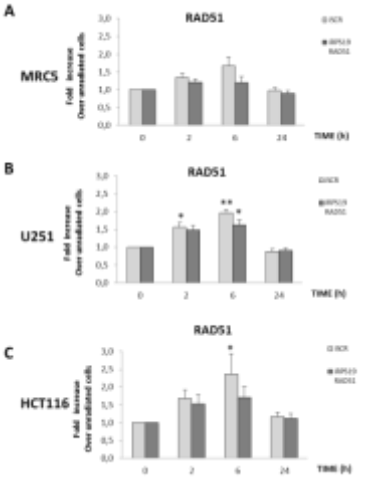

Fig. supplementary S12: RAD51 foci formation

MRC-5 (**A**), U251-MG (**B**) and HCT116 (**C**) were irradiated cells with 5 Gy of X-Rays, 48 or 72 hours after transfection. Number of foci was determined at 0 (unirradiated), 2, 6 and 24 hours after irradiation.

The graphs represent the fold induction of RAD51 foci of irradiated cells versus unirradiated cells. Error bars represent standard deviation of the mean calculated from minimum of three independent experiments.

Statistical analysis describes the fold induction of irradiated cells versus unradiated cells (*P<0.05, **P<0.01, ***P<0.001, Student's t-test).

(iSCR:control siRNA; iRPS19:transfection with siRPS19).

11. PUBBLICATION

Longo, A. and Antoccia, A. *Extra-ribosomal role of RPS19 in normal and tumor cell lines exposed to ionizing radiation.* Manuscript in preparation.